Modelling Magnetic Activity in the Sun

Tim Whitbread

Supervisor: Dr. Paul Bushby

Stage 4 2014/2015

Abstract

Observations of sunspots on the surface of the Sun have opened up investigations into the evolution of the solar magnetic field. It is now generally accepted that the Sun's magnetic field is maintained by a hydromagnetic dynamo. The main aim of this project was to model the dynamo process mathematically. We first derived a nonlinear system of partial differential equations (PDEs) for the magnetic field and the associated velocity perturbation. We then considered Fourier series expansions for the field components to reduce the model to a system of ordinary differential equations (ODEs). This enabled us to search for the critical value of the 'dynamo number', the key parameter for ensuring dynamo action occurs. We continued by solving the PDE model numerically and observed results that shared features with solar observations. The critical dynamo number also agreed with our analytical dynamo number. In order to replicate more of these features, particularly modulation, the two parameters in the model were varied and modulation was successfully observed.

Contents

1 Introduction

1.1 Features of the Sun

Since the 16$^{\text{th}}$ century, when heliocentrism started to gain popularity[a], mankind has generally believed that the Sun is at the centre of the solar system. It is no wonder then that scientists have been interested in the activity that occurs within and on the surface of the star that is crucial to our existence. Following the invention of the telescope, we have been able to directly observe the incidence of sunspots, which are cooler, darker areas of the Sun's surface attributed to regions of strong magnetic fields. The emergence of these sunspots follows a cycle with a period of approximately eleven years, and it has been conjectured that the cycle is maintained by a hydromagnetic dynamo. We have also observed convection in the form of granulation on the surface of the Sun, as shown in Figure 1. The lighter areas represent convective upflows, whilst the dark, thin lines represent convective downflows. This convection plays an important role in the dynamo.

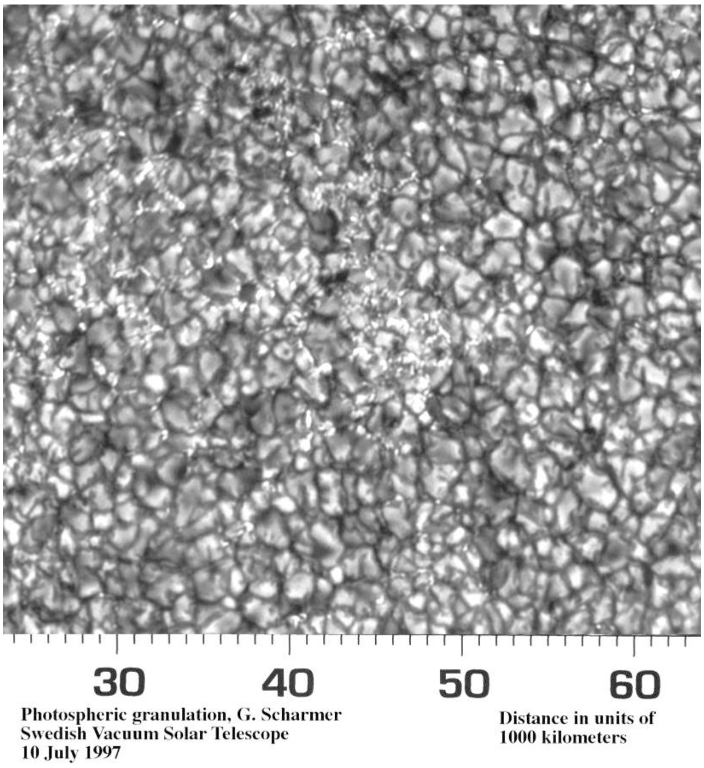

Figure 1: Granulation on the surface of the Sun indicating small-scale convection.
Taken from http://solarscience.msfc.nasa.gov

Much like the Earth, the Sun's interior is made up of different layers (Figure 2). In the centre is the core, which is responsible for the production of nuclear energy via the fusion of hydrogen to form helium. In the radiative zone, the energy generated in the core is transported outwards by radiation, before reaching the convection zone, where convective motions take control and transport the energy to the surface (Tobias, 2002). There is also a layer between the convective and radiative zones known as the tachocline which is believed to be where the magnetic field is created (Spiegel & Zahn, 1992). The tachocline will be discussed further in Section 2.

[a] http://www.universetoday.com/33113/heliocentric-model/

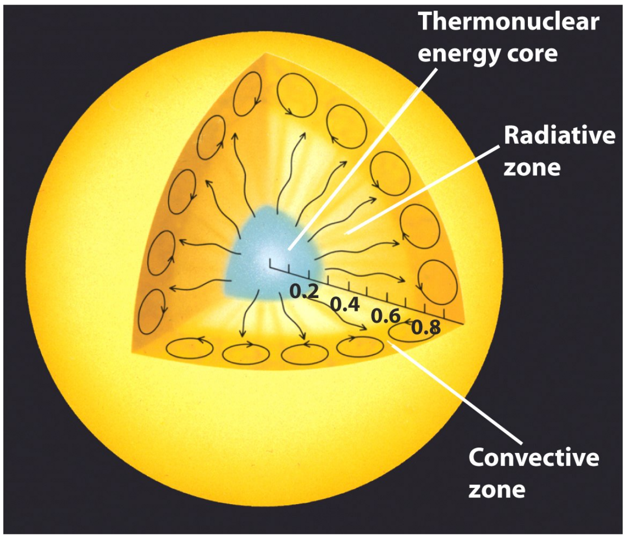

Figure 2: The solar interior. Energy is transported radially outwards due to radiation before convective motions take over at approximately $0.7R_{\odot}$. Taken from http://tuttidentro.files.wordpress.com

An aspect of the Sun which is key to understanding the solar dynamo is differential rotation. Through helioseismology, which is the study of acoustic wave oscillations in the Sun, it has been shown (for example, by Schou *et al.* (1998)) that the Sun rotates with different angular velocities at different latitudes; at the equator, the rotation rate is higher than that of the poles. This is the case throughout the convection zone, though it appears that the radiative zone rotates as a solid body. Figure 3 is a cross-section of the Sun which shows the rotation rate at different latitudes and at different depths. The dashed line is the location of the tachocline, and radially below this is the radiative zone, which appears to rotate at approximately the same rate throughout. It is not clear why this is true, but it may be due to the internal magnetic field which could enforce rigid body rotation.

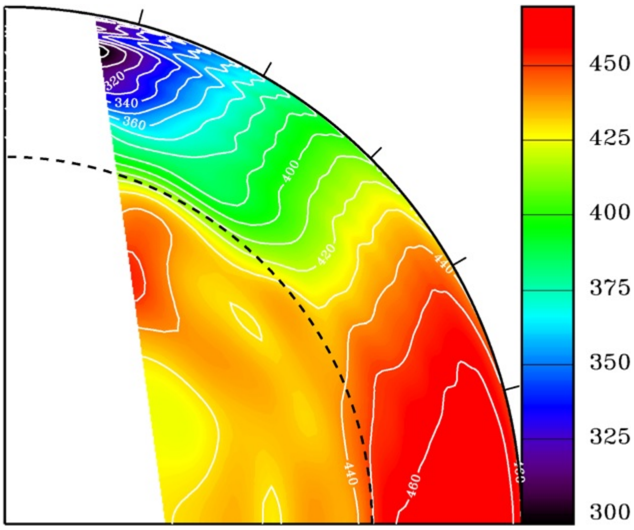

Figure 3: Differential rotation in the Sun. Rotation rate is higher at the equator than at the poles. The frequency is measured in nHz and the dashed line represents the base of the convection zone. Taken from Schou *et al.* (1998)

1.2 Observations

As mentioned in Section 1.1, the occurrence of sunspots has been investigated over the past few centuries. Figure 4 is the so-called 'butterfly diagram', showing the latitudinal position of sunspots over time for the last 130 years. It appears that sunspots occur on a cycle of approximately 11 years, a cycle which is now known as 'the solar cycle' and first noticed in 1843 by Samuel Heinrich Schwabe (Hoyt & Schatten, 1997). At the start of the cycle, sunspots begin to appear at latitudes of ±30°, then the emergence positions migrate towards the equator over the next 11 years. Furthermore, the leading spots in the northern hemisphere have an opposite polarity to those in the southern hemisphere. At the end of the cycle, the field reverses and the polarities are flipped for the next cycle (Hale, 1924).

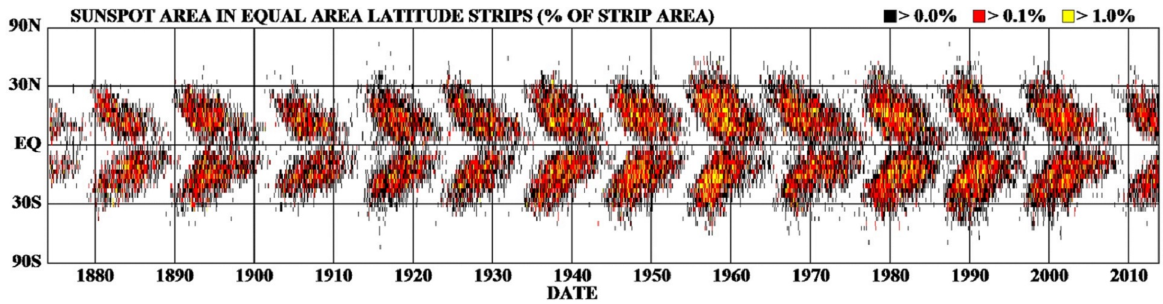

Figure 4: Butterfly diagram showing equatorward migration of sunspots. Taken from http://solarscience.msfc.nasa.gov

We can also use the sunspot number to investigate solar magnetic activity. Figure 5 is an example of a plot of sunspot number versus time. The sunspot number seems largely unpredictable, but what is striking is the lack of sunspots between 1650–1700. This wasn't a period of fewer records or lack of interest in the Sun, but a genuine phenomenon where magnetic activity was at a minimum. This period of magnetic inactivity is known as the 'Maunder Minimum' (Eddy, 1976). Moreover, as the Maunder Minimum came to an end, sunspots were only observed in the southern hemisphere, until that cycle finished and the sunspots returned to occupying both hemispheres non-preferentially.

In order to examine magnetic activity that occurred thousands of years ago, we can analyse proxy data to see if the solar cycle has been following the same 11 year pattern, or indeed if any other grand minima like the Maunder Minimum have occurred. The interaction of cosmic ray flux entering the earth with the solar magnetic field results in the production of ^{10}Be and ^{14}C, which can be found in polar icecaps and tree rings respectively. The abundances of these can therefore be used to deduce solar magnetic activity over the past few millennia. It was found that the abundances are anti-correlated with magnetic activity, and that grand minima have in fact occurred before on multiple occasions, with a mean period of approximately 200 years (Beer, 2000). In addition, during the Maunder Minimum the magnetic activity persisted but at a decreased level and with a shorter cycle (Beer *et al.*, 1998).

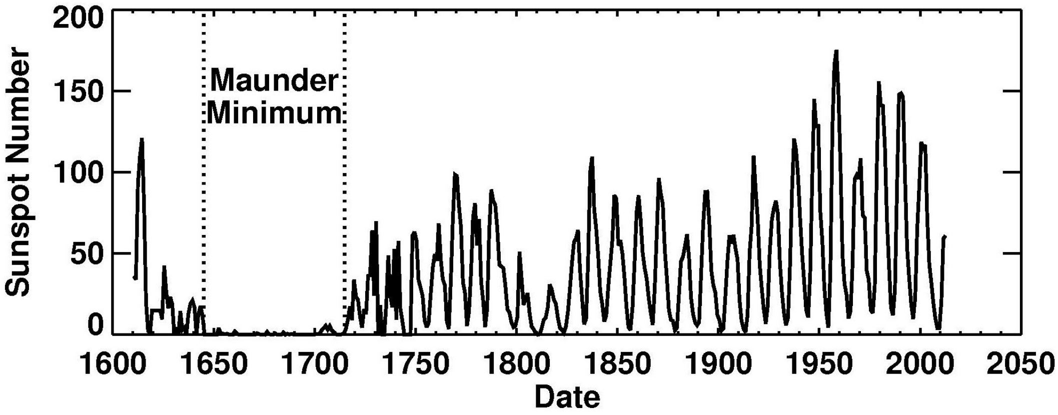

Figure 5: Sunspot number over time. The Maunder Minimum was a period of decreased magnetic activity. Taken from http://solarscience.msfc.nasa.gov

2 Basics of the Dynamo

Now we investigate how the dynamo process works. We start by recognising that the Sun's magnetic field is made up of two components, namely the toroidal (azimuthal) field and the poloidal (meridional) field. The dynamo process is then based around the regeneration of the two components of the field, and in fact it turns out that one is produced from the other. Figure 6 is an illustrative representation of the dynamo cycle described below.

Firstly we consider the poloidal field under the effect of differential rotation, which was discussed in Section 1.1. The rotation with higher frequency at the equator stretches the field azimuthally to create a toroidal field. This is known as the ω-effect. The converse to this, however, is more complicated. Parker (1955a) suggested that the toroidal field is stretched by convective upwellings then twisted by the Coriolis effect to form small-scale poloidal loops. These loops then come together to form a large-scale poloidal field. This is known as the α-effect. The α-effect has since been constructed mathematically using 'mean-field electrodynamics', which will be shown in Section 3.

We now need to explain whereabouts in the Sun this process is occurring. The effects of differential rotation and convection, which are used to produce the toroidal and poloidal components of the magnetic field respectively, are both observed in the convective zone of the solar interior. However, regions of high magnetic flux are less dense than their surroundings and hence become buoyant (Parker, 1955b), meaning they would rise to the surface on a shorter timescale than the cycle of 11 years which we observe from the butterfly diagrams. Furthermore, the diffusion rate in the turbulent convection zone may be too strong for field to be generated. Instead, turbulent pumping sends the magnetic flux to the tachocline at the base of the convection zone (Tobias *et al.*, 1998), where the effect of differential rotation is at its strongest and the turbulent diffusion effect is smaller. The poloidal field is stretched into toroidal field, and this is transported back to the convection zone by magnetic buoyancy and diffusion, where it is in turn deformed by the α-effect to produce poloidal field. The poloidal field is carried down to the tachocline again and the cycle continues. Only the strongest magnetic field will be carried to the surface to form sunspots. It seems sensible therefore to place the dynamo at the base of the convection zone.

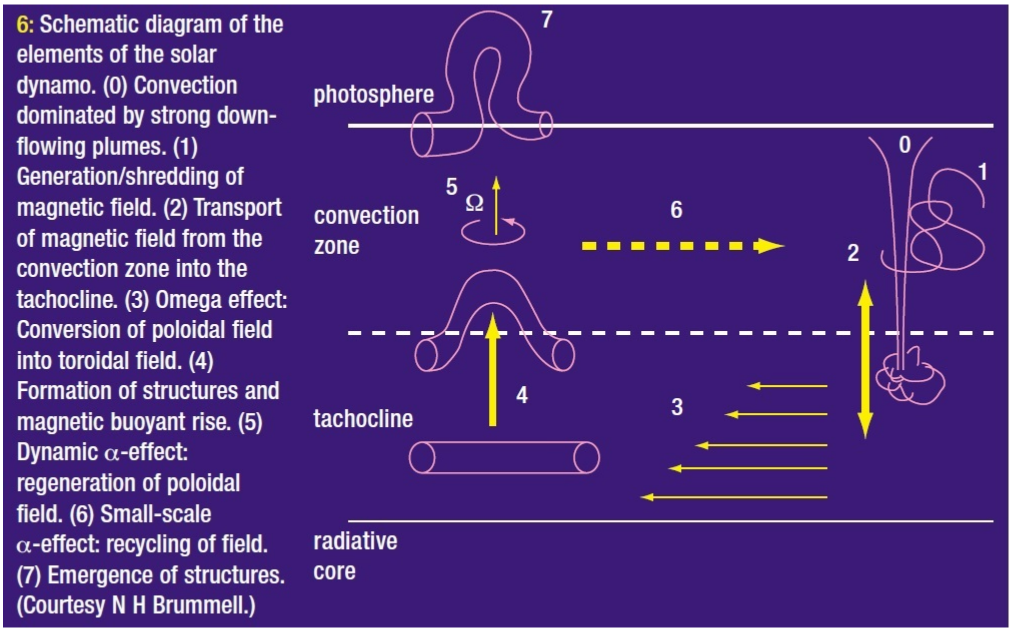

Figure 6: A sketch outlining the dynamo process. Taken from Bushby & Mason (2004)

3 Deriving a Model

3.1 The Induction Equation

After discussing key features of the Sun and the dynamo process, we can now derive equations to model the Sun's magnetic activity. We start by deriving the induction equation from the pre-Maxwell equations:

$$\nabla \times \mathbf{B} = \mu_0 \mathbf{j}, \tag{3.1}$$

$$\nabla \cdot \mathbf{B} = 0, \tag{3.2}$$

$$\nabla \times \mathbf{E} = -\frac{\partial \mathbf{B}}{\partial t}, \tag{3.3}$$

and Ohm's Law in a moving medium,

$$\mathbf{j} = \sigma \left(\mathbf{E} + \mathbf{u} \times \mathbf{B} \right), \tag{3.4}$$

where μ_0 and σ are constants.

From Ohm's Law,

$$\begin{aligned} \nabla \times \mathbf{j} &= \sigma \left(\nabla \times \mathbf{E} + \nabla \times (\mathbf{u} \times \mathbf{B}) \right) && (3.5) \\ &= \sigma \left(-\frac{\partial \mathbf{B}}{\partial t} + \nabla \times (\mathbf{u} \times \mathbf{B}) \right). && (3.6) \end{aligned}$$

Also we have

$$\nabla \times (\nabla \times \mathbf{B}) = \mu_0 (\nabla \times \mathbf{j}), \tag{3.7}$$

and so we can use the identity $\nabla \times (\nabla \times \mathbf{A}) = \nabla (\nabla \cdot \mathbf{A}) - \nabla^2 \mathbf{A}$ (see Section 9) to get

$$\nabla \times (\nabla \times \mathbf{B}) = -\nabla^2 \mathbf{B}, \tag{3.8}$$

since $\nabla \cdot \mathbf{B} = 0$.

Putting this together, we have:

$$-\frac{1}{\mu_0 \sigma} \nabla^2 \mathbf{B} = -\frac{\partial \mathbf{B}}{\partial t} + \nabla \times (\mathbf{u} \times \mathbf{B}) \tag{3.9}$$

$$\Rightarrow \qquad \frac{\partial \mathbf{B}}{\partial t} = \nabla \times (\mathbf{u} \times \mathbf{B}) + \eta \nabla^2 \mathbf{B}, \tag{3.10}$$

where $\eta = \dfrac{1}{\mu_0 \sigma}$ is constant.

This is the induction equation.

3.2 The Mean-Field Dynamo Equation

Now we can decompose $\mathbf{B}$ and $\mathbf{u}$ into mean and fluctuating parts, with $\langle . \rangle$ representing the averaging operator:

$$\mathbf{B} = \mathbf{B}_0 + \mathbf{B}', \tag{3.11}$$

$$\mathbf{u} = \mathbf{u}_0 + \mathbf{u}', \tag{3.12}$$

where $\mathbf{B}_0 = \langle \mathbf{B} \rangle$, $\mathbf{u}_0 = \langle \mathbf{u} \rangle$, $\langle \mathbf{B}' \rangle = \langle \mathbf{u}' \rangle = \mathbf{0}$.

Then

$$\frac{\partial}{\partial t} (\mathbf{B}_0 + \mathbf{B}') = \nabla \times ((\mathbf{u}_0 + \mathbf{u}') \times (\mathbf{B}_0 + \mathbf{B}')) + \eta \nabla^2 (\mathbf{B}_0 + \mathbf{B}') \tag{3.13}$$

$$= \nabla \times ((\mathbf{u}_0 \times \mathbf{B}_0) + (\mathbf{u}_0 \times \mathbf{B}') + (\mathbf{u}' \times \mathbf{B}_0) + (\mathbf{u}' \times \mathbf{B}')) + \eta \nabla^2 (\mathbf{B}_0 + \mathbf{B}'). \tag{3.14}$$

Taking the average of this, we get:

$$\frac{\partial \mathbf{B}_0}{\partial t} = \nabla \times (\mathbf{u}_0 \times \mathbf{B}_0) + \nabla \times (\mathbf{u}_0 \times \langle \mathbf{B}' \rangle) + \nabla \times (\langle \mathbf{u}' \rangle \times \mathbf{B}_0) + \nabla \times \langle \mathbf{u}' \times \mathbf{B}' \rangle + \eta \nabla^2 \mathbf{B}_0 \tag{3.15}$$

$$= \nabla \times (\mathbf{u}_0 \times \mathbf{B}_0) + \nabla \times \langle \mathbf{u}' \times \mathbf{B}' \rangle + \eta \nabla^2 \mathbf{B}_0. \tag{3.16}$$

This is an evolution equation for the mean magnetic field.

Subtracting this from Equation 3.10, we obtain:

$$\frac{\partial \mathbf{B}'}{\partial t} = \nabla \times ((\mathbf{u}_0 \times \mathbf{B}') + (\mathbf{u}' \times \mathbf{B}_0) + (\mathbf{u}' \times \mathbf{B}') - \langle \mathbf{u}' \times \mathbf{B}' \rangle) + \eta \nabla^2 \mathbf{B}'. \tag{3.17}$$

If the flow is prescribed, this implies that $\mathbf{B}'$ is linearly related to $\mathbf{B}_0$, i.e. $\langle \mathbf{u}' \times \mathbf{B}' \rangle$ is linearly related to $\mathbf{B}_0$. Therefore we can assume a relation of the form

$$\langle \mathbf{u}' \times \mathbf{B}' \rangle_i = \alpha_{ij} B_{0j} + \beta_{ijk} \frac{\partial B_{0j}}{\partial x_k} + \text{higher order terms.} \tag{3.18}$$

We consider the case of homogeneous isotropic turbulence, so we can write

$$\alpha_{ij} = \alpha \delta_{ij}, \tag{3.19}$$

$$\beta_{ijk} = \beta \epsilon_{ijk}, \tag{3.20}$$

then

$$\begin{aligned} \langle \mathbf{u}' \times \mathbf{B}' \rangle_i &= \alpha \delta_{ij} B_{0j} + \beta \epsilon_{ijk} \frac{\partial B_{0j}}{\partial x_k} + \ldots & (3.21) \\ &= \alpha B_{0i} - \beta \epsilon_{ikj} \frac{\partial B_{0k}}{\partial x_j} + \ldots & (3.22) \\ &= \alpha B_{0i} - [\nabla \times \mathbf{B}_0]_i + \ldots & (3.23) \end{aligned}$$

Hence

$$\langle \mathbf{u}' \times \mathbf{B}' \rangle \approx \alpha \mathbf{B}_0 - \beta \nabla \times \mathbf{B}_0. \tag{3.24}$$

We can substitute this into Equation 3.16 to obtain:

$$\frac{\partial \mathbf{B}_0}{\partial t} = \nabla \times (\mathbf{u}_0 \times \mathbf{B}_0) + \nabla \times (\alpha \mathbf{B}_0) - \nabla \times (\beta \nabla \times \mathbf{B}_0) + \eta \nabla^2 \mathbf{B}_0. \tag{3.25}$$

Now we use the identity $\nabla \times (\phi \mathbf{A}) = \phi \nabla \times \mathbf{A} + (\nabla \phi) \times \mathbf{A}$, where $\phi(\mathbf{x})$ is a scalar function (see Section 9):

$$\begin{aligned} \nabla \times (\beta \nabla \times \mathbf{B}_0) &= \beta \nabla \times (\nabla \times \mathbf{B}_0) + (\nabla \beta) \times (\nabla \times \mathbf{B}_0) & (3.26) \\ &= \beta \left(\nabla (\nabla \cdot \mathbf{B}_0) - \nabla^2 \mathbf{B}_0 \right) + (\nabla \beta) \times (\nabla \times \mathbf{B}_0) & (3.27) \\ &= -\beta \nabla^2 \mathbf{B}_0 + (\nabla \beta) \times (\nabla \times \mathbf{B}_0), & (3.28) \end{aligned}$$

since

$$\begin{aligned} \nabla \cdot \mathbf{B} = 0 &\Rightarrow \langle \nabla \cdot \mathbf{B} \rangle = 0 \\ &\Rightarrow \nabla \cdot \langle \mathbf{B} \rangle = 0 \\ &\Rightarrow \nabla \cdot \mathbf{B}_0 = 0, \end{aligned}$$

so

$$\frac{\partial \mathbf{B}_0}{\partial t} = \nabla \times (\mathbf{u}_0 \times \mathbf{B}_0) + \nabla \times (\alpha \mathbf{B}_0) + (\eta + \beta) \nabla^2 \mathbf{B}_0 - (\nabla \beta) \times (\nabla \times \mathbf{B}_0). \tag{3.29}$$

This is the mean-field dynamo equation. The $\alpha \mathbf{B}_0$ term represents the α-effect, and β is the turbulent diffusivity which enhances the magnetic diffusivity.

3.3 Cartesian Model

We can write the magnetic field as

$$\mathbf{B}_0 = B\left(x,z,t\right)\hat{\mathbf{y}} + \nabla\times\left(A\left(x,z,t\right)\hat{\mathbf{y}}\right), \tag{3.30}$$

where B is the toroidal component and A is the vector potential of the poloidal component of the field. We flatten out a thin shell at the base of the convection zone in order to use Cartesian coordinates, where z is in the radial direction, x runs from pole to pole and y is in the azimuthal direction. We assume axis symmetry so the magnetic field is not dependent on y. We also represent a shear flow:

$$\mathbf{u}_0 = V\left(x,z\right)\hat{\mathbf{y}}. \tag{3.31}$$

For simplicity we consider β to be a constant, and let $\eta+\beta=\eta_T$. Also $\alpha\equiv\alpha\left(x,z\right)$. Then we substitute these into Equation 3.29:

$$\begin{aligned}\frac{\partial}{\partial t}\left(B\hat{\mathbf{y}}+\nabla\times A\hat{\mathbf{y}}\right) &= \nabla\times\left(V\hat{\mathbf{y}}\times\left(B\hat{\mathbf{y}}+\nabla\times A\hat{\mathbf{y}}\right)\right)\\ &\quad+\nabla\times\left(\alpha\left(B\hat{\mathbf{y}}+\nabla\times A\hat{\mathbf{y}}\right)\right)+\eta_T\nabla^2\left(B\hat{\mathbf{y}}+\nabla\times A\hat{\mathbf{y}}\right) \quad (3.32)\\ &= \nabla\times\left(V\hat{\mathbf{y}}\times B\hat{\mathbf{y}}\right)+\nabla\times\left(V\hat{\mathbf{y}}\times\left(\nabla\times A\hat{\mathbf{y}}\right)\right)\\ &\quad+\nabla\times\left(\alpha B\hat{\mathbf{y}}\right)+\nabla\times\left(\alpha\nabla\times A\hat{\mathbf{y}}\right)+\eta_T\nabla^2 B\hat{\mathbf{y}}\\ &\quad+\nabla\times\left(\eta_T\nabla^2 A\hat{\mathbf{y}}\right). \quad (3.33)\end{aligned}$$

Since $\hat{\mathbf{y}}\times\hat{\mathbf{y}}=\mathbf{0}$, we can see that

$$\nabla\times\left(V\hat{\mathbf{y}}\times B\hat{\mathbf{y}}\right)=\mathbf{0}. \tag{3.34}$$

Using vector calculus, it can also be shown that

$$\nabla\times\left(V\hat{\mathbf{y}}\times\left(\nabla\times A\hat{\mathbf{y}}\right)\right)=\left(\frac{\partial A}{\partial x}\frac{\partial V}{\partial z}-\frac{\partial A}{\partial z}\frac{\partial V}{\partial x}\right)\hat{\mathbf{y}}. \tag{3.35}$$

This term is more dominant than the $\nabla\times\left(\alpha\nabla\times A\hat{\mathbf{y}}\right)\cdot\hat{\mathbf{y}}$ term in the $\hat{\mathbf{y}}$ direction, so we can remove the latter. This is known as the $\alpha\omega$-approximation.

We also have:

$$\nabla\times\frac{\partial A\hat{\mathbf{y}}}{\partial t} = -\frac{\partial^2 A}{\partial z\partial t}\hat{\mathbf{x}}+\frac{\partial^2 A}{\partial x\partial t}\hat{\mathbf{z}}, \tag{3.36}$$

$$\nabla\times\left(\alpha B\hat{\mathbf{y}}\right) = -\frac{\partial}{\partial z}\left(\alpha B\right)\hat{\mathbf{x}}+\frac{\partial}{\partial x}\left(\alpha B\right)\hat{\mathbf{z}}, \tag{3.37}$$

$$\nabla\times\left(\eta_T\nabla^2 A\hat{\mathbf{y}}\right) = -\frac{\partial}{\partial z}\left(\eta_T\nabla^2 A\right)\hat{\mathbf{x}}+\frac{\partial}{\partial x}\left(\eta_T\nabla^2 A\right)\hat{\mathbf{z}}. \tag{3.38}$$

These give us three equations in the $\hat{\mathbf{x}}$, $\hat{\mathbf{y}}$ and $\hat{\mathbf{z}}$ directions respectively:

$$\frac{\partial}{\partial z}\left(\frac{\partial A}{\partial t}\right) = \frac{\partial}{\partial z}\left(\alpha B+\eta_T\nabla^2 A\right), \tag{3.39}$$

$$\frac{\partial B}{\partial t} = \frac{\partial A}{\partial x}\frac{\partial V}{\partial z}-\frac{\partial A}{\partial z}\frac{\partial V}{\partial x}+\eta_T\nabla^2 B, \tag{3.40}$$

$$\frac{\partial}{\partial x}\left(\frac{\partial A}{\partial t}\right) = \frac{\partial}{\partial x}\left(\alpha B+\eta_T\nabla^2 A\right). \tag{3.41}$$

After integrating Equations (3.39) and (3.41) with respect to z and excluding the functions of time which arise from this without loss of generality, we obtain equations for the poloidal and toroidal components respectively:

$$\frac{\partial A}{\partial t} = \alpha B + \eta_T \nabla^2 A, \tag{3.42}$$

$$\frac{\partial B}{\partial t} = \frac{\partial A}{\partial x}\frac{\partial V}{\partial z} - \frac{\partial A}{\partial z}\frac{\partial V}{\partial x} + \eta_T \nabla^2 B. \tag{3.43}$$

3.4 Linear Theory

First we follow the work of Parker (1955a) and seek z-independent solutions of the form:

$$A = \hat{A} e^{\sigma t + ikx}, \tag{3.44}$$

$$B = \hat{B} e^{\sigma t + ikx}, \tag{3.45}$$

where σ is a complex growth rate and k is a real wavenumber. Substituting these into the above equations, and letting α and $\frac{\partial V}{\partial z} \equiv V'$ be a constant, we obtain two equations for the growth rate:

$$\sigma \hat{A} = \alpha \hat{B} - \eta_T k^2 \hat{A}, \tag{3.46}$$

$$\sigma \hat{B} = ikV'\hat{A} - \eta_T k^2 \hat{B}. \tag{3.47}$$

These can be represented in matrix form:

$$\begin{pmatrix} \sigma + \eta_T k^2 & -\alpha \\ -ikV' & \sigma + \eta_T k^2 \end{pmatrix} \begin{pmatrix} \hat{A} \\ \hat{B} \end{pmatrix} = \begin{pmatrix} 0 \\ 0 \end{pmatrix}. \tag{3.48}$$

If this equation is to hold then the determinant must equal zero, i.e.,

$$\left(\sigma + \eta_T k^2\right)^2 - \alpha ikV' = 0 \tag{3.49}$$

$$\Rightarrow \qquad \sigma + \eta_T k^2 = \pm\sqrt{\alpha ikV'}, \tag{3.50}$$

and noting that $\sqrt{i} = \frac{1}{\sqrt{2}}(1+i)$, we can rearrange to get our final expression for the growth rate:

$$\sigma = -\eta_T k^2 \left(1 \pm (1+i)\sqrt{D}\right), \tag{3.51}$$

where $D = \dfrac{\alpha V'}{2\eta_T^2 k^3}$ is the so-called dynamo number.

For dynamo action to take place, we require the real part of σ to be greater than zero, so dynamo action will only occur when $|D| > 1$. Note that $\eta_T k^2 \sim \dfrac{1}{\tau_\eta}$, where τ_η is the ohmic decay time. We also see that the imaginary part of σ is non-zero, so we would expect oscillatory solutions at onset.

3.5 Introducing Nonlinearity

Now following the method of Tobias (1996), let

$$\mathbf{u}_0 = v(x,z)\,\hat{\mathbf{y}} + v'(x,z,t)\,\hat{\mathbf{y}}, \tag{3.52}$$

where v' is the fluctuating part of $\mathbf{u}_0$, and re-introduce z-dependence to A and B. Then v' obeys the Navier-Stokes equation:

$$\rho\left(\frac{\partial}{\partial t}v'\hat{\mathbf{y}} + (v'\hat{\mathbf{y}}\cdot\nabla)\,v'\hat{\mathbf{y}}\right) = [-\nabla p]_y + [\mathbf{j}\times\mathbf{B}_0]_y + \rho\nu\nabla^2 v'\hat{\mathbf{y}} + [\mathbf{F}]_y\,. \tag{3.53}$$

Firstly we see that $(v'\hat{\mathbf{y}}\cdot\nabla)\,v'\hat{\mathbf{y}} = 0$, since $v'\hat{\mathbf{y}}$ does not depend on y. Similarly, we assume that p does not depend on y, so $[-\nabla p]_y = 0$. The forces contained in $\mathbf{F}$, including gravity and turbulent stresses, determine the background velocity field and not the evolution of the magnetically-induced velocity perturbation which we are investigating here, so we can ignore it.

From Equation 3.1, we know that

$$\mathbf{j}\times\mathbf{B}_0 = \frac{1}{\mu_0}(\nabla\times\mathbf{B}_0)\times\mathbf{B}_0. \tag{3.54}$$

This nonlinear term represents the Lorentz force. Using vector calculus, we obtain:

$$[(\nabla\times\mathbf{B}_0)\times\mathbf{B}_0]_y = \frac{\partial A}{\partial x}\frac{\partial B}{\partial z} - \frac{\partial A}{\partial z}\frac{\partial B}{\partial x}. \tag{3.55}$$

Then our equation for v' in the $\hat{\mathbf{y}}$-direction is:

$$\frac{\partial v'}{\partial t} = \frac{1}{\rho\mu_0}\left(\frac{\partial A}{\partial x}\frac{\partial B}{\partial z} - \frac{\partial A}{\partial z}\frac{\partial B}{\partial x}\right) + \nu\nabla^2 v'. \tag{3.56}$$

3.6 Dimensionless Equations

We now have three equations which we can make dimensionless:

$$\frac{\partial A}{\partial t} = \alpha B + \eta_T\nabla^2 A, \tag{3.57}$$

$$\frac{\partial B}{\partial t} = \frac{\partial A}{\partial x}\frac{\partial}{\partial z}(v+v') - \frac{\partial A}{\partial z}\frac{\partial}{\partial x}(v+v') + \eta_T\nabla^2 B, \tag{3.58}$$

$$\frac{\partial v'}{\partial t} = \frac{1}{\rho\mu_0}\left(\frac{\partial A}{\partial x}\frac{\partial B}{\partial z} - \frac{\partial A}{\partial z}\frac{\partial B}{\partial x}\right) + \nu\nabla^2 v'. \tag{3.59}$$

We do this by introducing the following dimensionless variables:

$$\begin{gathered}\mathbf{x}\sim l\hat{\mathbf{x}},\quad \nabla\sim\frac{1}{l}\hat{\nabla},\quad \nabla^2\sim\frac{1}{l^2}\hat{\nabla}^2,\quad \eta_T\sim\eta_0\hat{\eta},\\ \nu\sim\nu_0\hat{\nu},\quad v\sim v_0\hat{v},\quad v'\sim v_0\hat{v}',\quad \alpha\sim\alpha_0\hat{\alpha}(x,z),\\ t\sim\frac{l^2}{\eta_0}\hat{t},\quad \frac{\partial}{\partial t}\sim\frac{\eta_0}{l^2}\frac{\partial}{\partial\hat{t}},\quad B\sim B_0\hat{B},\quad A\sim lB_0\hat{A}.\end{gathered} \tag{3.60}$$

Then our equations become:

$$\frac{\partial\hat{A}}{\partial\hat{t}} = R_\alpha\hat{\alpha}\hat{B} + \hat{\eta}\hat{\nabla}^2\hat{A}, \tag{3.61}$$

$$\frac{\partial\hat{B}}{\partial\hat{t}} = R_\omega\left(\frac{\partial\hat{A}}{\partial\hat{x}}\frac{\partial}{\partial\hat{z}}(\hat{v}+\hat{v}') - \frac{\partial\hat{A}}{\partial\hat{z}}\frac{\partial}{\partial\hat{x}}(\hat{v}+\hat{v}')\right) + \hat{\eta}\hat{\nabla}^2\hat{B}, \tag{3.62}$$

$$\frac{\partial\hat{v}'}{\partial\hat{t}} = \frac{lB_0^2}{\rho\mu_0 v_0\eta_0}\left(\frac{\partial\hat{A}}{\partial\hat{x}}\frac{\partial\hat{B}}{\partial\hat{z}} - \frac{\partial\hat{A}}{\partial\hat{z}}\frac{\partial\hat{B}}{\partial\hat{x}}\right) + P_m\hat{\nu}\hat{\nabla}^2\hat{v}', \tag{3.63}$$

where $R_\alpha = \dfrac{\alpha_0 l}{\eta_0}$, $R_\omega = \dfrac{l v_0}{\eta_0}$ and $P_m = \dfrac{\nu_0}{\eta_0}$ are dimensionless constants.

Now let $\hat{A} \sim R_\alpha A'$:

$$\frac{\partial A'}{\partial \hat{t}} = \hat{\alpha}\hat{B} + \hat{\eta}\hat{\nabla}^2 A', \tag{3.64}$$

$$\frac{\partial \hat{B}}{\partial \hat{t}} = D\left(\frac{\partial A'}{\partial \hat{x}}\frac{\partial}{\partial \hat{z}}(\hat{v}+\hat{v}') - \frac{\partial A'}{\partial \hat{z}}\frac{\partial}{\partial \hat{x}}(\hat{v}+\hat{v}')\right) + \hat{\eta}\hat{\nabla}^2\hat{B}, \tag{3.65}$$

$$\frac{\partial \hat{v}'}{\partial \hat{t}} = R_\alpha \frac{l B_0^2}{\rho\mu_0 v_0 \eta_0}\left(\frac{\partial A'}{\partial \hat{x}}\frac{\partial \hat{B}}{\partial \hat{z}} - \frac{\partial A'}{\partial \hat{z}}\frac{\partial \hat{B}}{\partial \hat{x}}\right) + P_m \hat{\nu}\hat{\nabla}^2 \hat{v}', \tag{3.66}$$

where $D = R_\alpha R_\omega$.

We let

$$\Lambda = \frac{l B_0^2}{\rho\mu_0 v_0 \eta_0}, \tag{3.67}$$

then

$$A' \sim |R_\alpha \Lambda|^{-\frac{1}{2}} A_*, \quad \hat{B} \sim |R_\alpha \Lambda|^{-\frac{1}{2}} B_*, \tag{3.68}$$

so

$$\frac{\partial \hat{v}'}{\partial \hat{t}} = \operatorname{sign}(R_\alpha \Lambda)\left(\frac{\partial A_*}{\partial \hat{x}}\frac{\partial B_*}{\partial \hat{z}} - \frac{\partial A_*}{\partial \hat{z}}\frac{\partial B_*}{\partial \hat{x}}\right) + P_m \hat{\nu}\hat{\nabla}^2 \hat{v}'. \tag{3.69}$$

But we note that

$$R_\alpha \Lambda = \frac{\alpha_0}{v_0} \cdot \frac{l^2 B_0^2}{\rho \mu_0 \eta_0^2}, \tag{3.70}$$

so the sign of $R_\alpha \Lambda$ is the same as the sign of $\dfrac{\alpha_0}{v_0}$. Furthermore,

$$D = \frac{\alpha_0 l^2 v_0}{\eta_0^2}, \tag{3.71}$$

so the sign of D is also the same as the sign of $\dfrac{\alpha_0}{v_0}$. Hence our three final dimensionless equations (removing symbols denoting dimensionless variables, and letting $\eta = \nu = 1$ for simplicity) are:

$$\frac{\partial A}{\partial t} = \alpha B + \nabla^2 A, \tag{3.72}$$

$$\frac{\partial B}{\partial t} = D\left(\frac{\partial A}{\partial x}\frac{\partial}{\partial z}(v+v') - \frac{\partial A}{\partial z}\frac{\partial}{\partial x}(v+v')\right) + \nabla^2 B, \tag{3.73}$$

$$\frac{\partial v'}{\partial t} = \operatorname{sign}(D)\left(\frac{\partial A}{\partial x}\frac{\partial B}{\partial z} - \frac{\partial A}{\partial z}\frac{\partial B}{\partial x}\right) + P_m \nabla^2 v'. \tag{3.74}$$

4 Reduction to One Spatial Dimension

We now divert from work done in previous papers to start using original methods to solve these equations. Initially we will reduce these equations to one spatial dimension by considering the following forms of A, B and v':

$$A \sim \hat{A}(x,t)\sin(\pi z), \tag{4.1}$$

$$B \sim \hat{B}(x,t)\sin(\pi z), \tag{4.2}$$

$$v' \sim \hat{v}'(x,t)\sin(2\pi z), \tag{4.3}$$

where $0 \leq z \leq 1$. This ensures that A, B and v' vanish at $z = 0$ and $z = 1$, a plausible assumption for a dynamo that is localised around the base of the convection zone. v' is written in terms of $\sin(2\pi z)$ to account for the fact that the Lorentz force is quadratic and will produce a term involving $\sin(\pi z)\cos(\pi z)$ which is proportional to $\sin(2\pi z)$. Also $\alpha \equiv \alpha(x)$, and $v \equiv v(z)$ such that $\dfrac{\partial v}{\partial z}$ is constant.

Then from Equation 3.72, we get:

$$\begin{aligned}\frac{\partial}{\partial t}\left(\hat{A}\sin(\pi z)\right) &= \alpha\hat{B}\sin(\pi z) + \frac{\partial^2}{\partial x^2}\left(\hat{A}\sin(\pi z)\right) + \frac{\partial^2}{\partial z^2}\left(\hat{A}\sin(\pi z)\right)\\ &= \alpha\hat{B}\sin(\pi z) + \frac{\partial^2\hat{A}}{\partial x^2}\sin(\pi z) - \pi^2\hat{A}\sin(\pi z).\end{aligned} \tag{4.4}$$

Then projecting onto the relevant Fourier mode, the equation for $\hat{A}$ is:

$$\frac{\partial\hat{A}}{\partial t} = \alpha\hat{B} + \frac{\partial^2\hat{A}}{\partial x^2} - \pi^2\hat{A}. \tag{4.5}$$

Similarly from Equation 3.73 we get:

$$\begin{aligned}\frac{\partial}{\partial t}\left(\hat{B}\sin(\pi z)\right) &= D\Bigg(\frac{\partial}{\partial x}\left(\hat{A}\sin(\pi z)\right)\frac{\partial}{\partial z}\left(v + \hat{v}'\sin(2\pi z)\right)\\ &\quad - \frac{\partial}{\partial z}\left(\hat{A}\sin(\pi z)\right)\frac{\partial}{\partial x}\left(v + \hat{v}'\sin(2\pi z)\right)\Bigg)\\ &\quad + \frac{\partial^2}{\partial x^2}\left(\hat{B}\sin(\pi z)\right) + \frac{\partial^2}{\partial z^2}\left(\hat{B}\sin(\pi z)\right)\\ &= D\Bigg(\frac{\partial\hat{A}}{\partial x}\sin(\pi z)\frac{\partial v}{\partial z} + \frac{\partial\hat{A}}{\partial x}\sin(\pi z)\,2\pi\hat{v}'\cos(2\pi z)\\ &\quad - \pi\hat{A}\cos(\pi z)\frac{\partial\hat{v}'}{\partial x}\sin(2\pi z)\Bigg) + \frac{\partial^2\hat{B}}{\partial x^2}\sin(\pi z)\\ &\quad - \pi^2\hat{B}\sin(\pi z).\end{aligned} \tag{4.6}$$

Thus

$$\frac{\partial\hat{B}}{\partial t} = D\left(\frac{\partial\hat{A}}{\partial x}\frac{\partial v}{\partial z} - \pi\hat{v}'\frac{\partial\hat{A}}{\partial x} - \frac{\pi}{2}\hat{A}\frac{\partial\hat{v}'}{\partial x}\right) + \frac{\partial^2\hat{B}}{\partial x^2} - \pi^2\hat{B}, \tag{4.7}$$

since

$$\sin(3\pi z) + \sin(\pi z) = 2\sin(2\pi z)\cos(\pi z),$$

and

$$\sin(3\pi z) - \sin(\pi z) = 2\sin(\pi z)\cos(2\pi z).$$

Finally, from Equation 3.74 we obtain:

$$\begin{aligned}
\frac{\partial}{\partial t}\left(\hat{v}'\sin(2\pi z)\right) &= \operatorname{sign}(D)\left(\frac{\partial}{\partial x}\left(\hat{A}\sin(\pi z)\right)\frac{\partial}{\partial z}\left(\hat{B}\sin(\pi z)\right)\right. \\
&\quad \left. - \frac{\partial}{\partial z}\left(\hat{A}\sin(\pi z)\right)\frac{\partial}{\partial x}\left(\hat{B}\sin(\pi z)\right)\right) \\
&\quad + P_m\left(\frac{\partial^2}{\partial x^2}\left(\hat{v}'\sin(2\pi z)\right) + \frac{\partial^2}{\partial x^2}\left(\hat{v}'\sin(2\pi z)\right)\right) \\
&= \operatorname{sign}(D)\left(\frac{\partial \hat{A}}{\partial x}\sin(\pi z)\,\hat{B}\pi\cos(\pi z) - \pi\hat{A}\cos(\pi z)\frac{\partial \hat{B}}{\partial x}\sin(\pi z)\right) \\
&\quad + P_m\left(\frac{\partial^2 \hat{v}'}{\partial x^2}\sin(2\pi z) - 4\pi^2\hat{v}'\sin(2\pi z)\right). \qquad (4.8)
\end{aligned}$$

So

$$\frac{\partial \hat{v}'}{\partial t} = \operatorname{sign}(D)\left(\frac{\pi}{2}\hat{B}\frac{\partial \hat{A}}{\partial x} - \frac{\pi}{2}\hat{A}\frac{\partial \hat{B}}{\partial x}\right) + P_m\left(\frac{\partial^2 \hat{v}'}{\partial x^2} - 4\pi^2\hat{v}'\right), \qquad (4.9)$$

since

$$\sin(2\pi z) = 2\sin(\pi z)\cos(\pi z).$$

Hence, after reverting back to using A, B and v', the final three equations which form a model for the solar dynamo are:

$$\frac{\partial A}{\partial t} = \alpha B + \frac{\partial^2 A}{\partial x^2} - \pi^2 A, \qquad (4.10)$$

$$\frac{\partial B}{\partial t} = D\left(\frac{\partial A}{\partial x}\frac{\partial v}{\partial z} - \pi v'\frac{\partial A}{\partial x} - \frac{\pi}{2}A\frac{\partial v'}{\partial x}\right) + \frac{\partial^2 B}{\partial x^2} - \pi^2 B, \qquad (4.11)$$

$$\frac{\partial v'}{\partial t} = \operatorname{sign}(D)\frac{\pi}{2}\left(B\frac{\partial A}{\partial x} - A\frac{\partial B}{\partial x}\right) + P_m\left(\frac{\partial^2 v'}{\partial x^2} - 4\pi^2 v'\right). \qquad (4.12)$$

These can be solved numerically.

5 Reduction to ODE Model

Following an approach similar to that described by Bushby (2003) we express A, B and v' as Fourier sine series:

$$A(x,t) = \sum_{n=1}^{N} A_n(t)\sin\left(\frac{n\pi x}{L}\right), \qquad (5.1)$$

$$B(x,t) = \sum_{n=1}^{N} B_n(t)\sin\left(\frac{n\pi x}{L}\right), \qquad (5.2)$$

$$v'(x,t) = \sum_{n=1}^{N} v'_n(t)\sin\left(\frac{n\pi x}{L}\right). \qquad (5.3)$$

This means that the system can be reduced to set of ordinary differential equations which can be solved numerically and potentially even analytically. Sine series are chosen so that A, B and v' vanish at $x = 0$ and $x = L$. Initially we focus on $N = 2$ modes. Whilst this ensures easier calculation, a more realistic expansion is likely to involve more modes, since adding modes in a Fourier series induces convergence to a more accurate solution. For simplicity we set $\frac{\partial v}{\partial z}$ to be equal to unity. We also set $\alpha(x) = \cos\left(\frac{\pi x}{L}\right)$ so that the α-effect is strongest at the poles and vanishes at the equator, mimicking the α-effect on the Sun. Substituting these series into Equation 4.10 we obtain:

$$\begin{aligned}\frac{\partial A}{\partial t} = \frac{\partial A_1}{\partial t}\sin\left(\frac{\pi x}{L}\right) + \frac{\partial A_2}{\partial t}\sin\left(\frac{2\pi x}{L}\right) &= \cos\left(\frac{\pi x}{L}\right)\left(B_1\sin\left(\frac{\pi x}{L}\right) + B_2\sin\left(\frac{2\pi x}{L}\right)\right)\\ &- \frac{\pi^2}{L^2}A_1\sin\left(\frac{\pi x}{L}\right) - \frac{4\pi^2}{L^2}A_2\sin\left(\frac{2\pi x}{L}\right)\\ &- \pi^2\left(A_1\sin\left(\frac{\pi x}{L}\right) + A_2\sin\left(\frac{2\pi x}{L}\right)\right). \end{aligned} \tag{5.4}$$

Integrating this over the first Fourier mode, we get

$$\frac{dA_1}{dt} = \frac{1}{2}B_2 - \pi^2\left(1 + \frac{1}{L^2}\right)A_1, \tag{5.5}$$

and integrating over the second mode produces

$$\frac{dA_2}{dt} = \frac{1}{2}B_1 - \pi^2\left(1 + \frac{4}{L^2}\right)A_2. \tag{5.6}$$

Then we can insert the Fourier expansions into Equation 4.11 to obtain:

$$\begin{aligned}\frac{\partial B}{\partial t} = \; & D\Bigg(\left(\frac{\pi}{L}A_1\cos\left(\frac{\pi x}{L}\right) + \frac{2\pi}{L}A_2\cos\left(\frac{2\pi x}{L}\right)\right) - \frac{\pi^2}{L}v_1'A_1\sin\left(\frac{\pi x}{L}\right)\cos\left(\frac{\pi x}{L}\right)\\ & - \frac{2\pi^2}{L}v_1'A_2\sin\left(\frac{\pi x}{L}\right)\cos\left(\frac{2\pi x}{L}\right) - \frac{\pi^2}{L}v_2'A_1\sin\left(\frac{2\pi x}{L}\right)\cos\left(\frac{\pi x}{L}\right)\\ & - \frac{2\pi^2}{L}v_2'A_2\sin\left(\frac{2\pi x}{L}\right)\cos\left(\frac{2\pi x}{L}\right) - \frac{\pi^2}{2L}A_1v_1'\sin\left(\frac{\pi x}{L}\right)\cos\left(\frac{\pi x}{L}\right)\\ & - \frac{\pi^2}{L}A_1v_2'\sin\left(\frac{\pi x}{L}\right)\cos\left(\frac{2\pi x}{L}\right) - \frac{\pi^2}{2L}A_2v_1'\sin\left(\frac{2\pi x}{L}\right)\cos\left(\frac{\pi x}{L}\right)\\ & - \frac{\pi^2}{L}A_2v_2'\sin\left(\frac{2\pi x}{L}\right)\cos\left(\frac{2\pi x}{L}\right)\Bigg) - \left(\frac{\pi^2}{L^2}B_1\sin\left(\frac{\pi x}{L}\right) + \frac{4\pi^2}{L^2}B_2\sin\left(\frac{2\pi x}{L}\right)\right)\\ & - \pi^2\left(B_1\sin\left(\frac{\pi x}{L}\right) + B_2\sin\left(\frac{2\pi x}{L}\right)\right). \end{aligned} \tag{5.7}$$

Integrating over the first Fourier mode gives

$$\frac{dB_1}{dt} = D\left(-\frac{8}{3L}A_2 + \frac{3\pi^2}{4L}v_1'A_2\right) - \pi^2\left(1 + \frac{1}{L^2}\right)B_1, \tag{5.8}$$

where we have used

$$\int_0^L \sin\left(\frac{\pi x}{L}\right)\cos\left(\frac{2\pi x}{L}\right)dx = -\frac{2L}{3\pi},$$

and integrating over the second mode gives

$$\frac{dB_2}{dt} = D\left(\frac{8}{3L}A_1 - \frac{3\pi^2}{4L}v_1'A_1\right) - \pi^2\left(1+\frac{4}{L^2}\right)B_2, \tag{5.9}$$

where we have used

$$\int_0^L \sin\left(\frac{2\pi x}{L}\right)\cos\left(\frac{\pi x}{L}\right)dx = \frac{4L}{3\pi}.$$

Finally, we insert the expansions into Equation 4.12:

$$\begin{aligned}
\frac{\partial v'}{\partial t} \quad = \quad & \operatorname{sign}(D)\Bigg(\frac{\pi^2}{2L}B_1A_1\sin\left(\frac{\pi x}{L}\right)\cos\left(\frac{\pi x}{L}\right) + \frac{\pi^2}{L}B_1A_2\sin\left(\frac{\pi x}{L}\right)\cos\left(\frac{2\pi x}{L}\right)\\
&+ \frac{\pi^2}{2L}B_2A_1\sin\left(\frac{2\pi x}{L}\right)\cos\left(\frac{\pi x}{L}\right) + \frac{\pi^2}{L}B_2A_2\sin\left(\frac{2\pi x}{L}\right)\cos\left(\frac{2\pi x}{L}\right)\\
&- \frac{\pi^2}{2L}A_1B_1\sin\left(\frac{\pi x}{L}\right)\cos\left(\frac{\pi x}{L}\right) - \frac{\pi^2}{L}A_1B_2\sin\left(\frac{\pi x}{L}\right)\cos\left(\frac{2\pi x}{L}\right)\\
&- \frac{\pi^2}{2L}A_2B_1\sin\left(\frac{2\pi x}{L}\right)\cos\left(\frac{\pi x}{L}\right) - \frac{\pi^2}{L}A_2B_2\sin\left(\frac{2\pi x}{L}\right)\cos\left(\frac{2\pi x}{L}\right)\Bigg)\\
&+ P_m\Bigg(-\frac{\pi^2}{L^2}v_1'\sin\left(\frac{\pi x}{L}\right) - \frac{4\pi^2}{L^2}v_2'\sin\left(\frac{2\pi x}{L}\right)\\
&- 4\pi^2\left(v_1'\sin\left(\frac{\pi x}{L}\right) + v_2'\sin\left(\frac{2\pi x}{L}\right)\right)\Bigg).
\end{aligned} \tag{5.10}$$

We integrate over the first Fourier mode to obtain:

$$\frac{dv_1'}{dt} = \operatorname{sign}(D)\frac{3\pi^2}{4L}(A_1B_2 - A_2B_1) - P_m\pi^2\left(4+\frac{1}{L^2}\right)v_1', \tag{5.11}$$

and we integrate over the second Fourier mode to obtain:

$$\frac{dv_2'}{dt} = -4P_m\pi^2\left(1+\frac{1}{L^2}\right)v_2'. \tag{5.12}$$

Hence the six equations that form our ODE model are:

$$\frac{dA_1}{dt} = \frac{1}{2}B_2 - \pi^2\left(1+\frac{1}{L^2}\right)A_1, \tag{5.13}$$

$$\frac{dA_2}{dt} = \frac{1}{2}B_1 - \pi^2\left(1+\frac{4}{L^2}\right)A_2, \tag{5.14}$$

$$\frac{dB_1}{dt} = D\left(-\frac{8}{3L}A_2 + \frac{3\pi^2}{4L}v_1'A_2\right) - \pi^2\left(1+\frac{1}{L^2}\right)B_1, \tag{5.15}$$

$$\frac{dB_2}{dt} = D\left(\frac{8}{3L}A_1 - \frac{3\pi^2}{4L}v_1'A_1\right) - \pi^2\left(1+\frac{4}{L^2}\right)B_2, \tag{5.16}$$

$$\frac{dv_1'}{dt} = \operatorname{sign}(D)\frac{3\pi^2}{4L}(A_1B_2 - A_2B_1) - P_m\pi^2\left(4+\frac{1}{L^2}\right)v_1', \tag{5.17}$$

$$\frac{dv_2'}{dt} = -4P_m\pi^2\left(1+\frac{1}{L^2}\right)v_2'. \tag{5.18}$$

We note that Equation 5.18 is dependent on v_2' only, so this decouples from the rest of the system and we can remove this from consideration. Furthermore, the solution to the equation is

$$v_2' = Ke^{-4P_m\pi^2\left(1+\frac{1}{L^2}\right)t}, \tag{5.19}$$

where K is a constant, and this decays over time.

We now seek a fixed state, i.e., where $\frac{d}{dt} = 0$. We see that the trivial case is $A_1 = A_2 = B_1 = B_2 = v_1' = 0$. We perturb the state by assuming the following forms:

$$A_1 = \hat{A}_1, \quad A_2 = \hat{A}_2, \quad B_1 = \hat{B}_1, \quad B_2 = \hat{B}_2, \quad v_1' = \hat{v_1}', \tag{5.20}$$

where $\hat{:}$ denotes a small perturbation. We substitute these into our ODE model and linearise the system by removing any nonlinear terms. This leaves us with the following equations:

$$\frac{d\hat{A}_1}{dt} = \frac{1}{2}\hat{B}_2 - \pi^2\left(1+\frac{1}{L^2}\right)\hat{A}_1, \tag{5.21}$$

$$\frac{d\hat{A}_2}{dt} = \frac{1}{2}\hat{B}_1 - \pi^2\left(1+\frac{4}{L^2}\right)\hat{A}_2, \tag{5.22}$$

$$\frac{d\hat{B}_1}{dt} = -\frac{8D}{3L}\hat{A}_2 - \pi^2\left(1+\frac{1}{L^2}\right)\hat{B}_1, \tag{5.23}$$

$$\frac{d\hat{B}_2}{dt} = \frac{8D}{3L}\hat{A}_1 - \pi^2\left(1+\frac{4}{L^2}\right)\hat{B}_2, \tag{5.24}$$

$$\frac{d\hat{v_1}'}{dt} = -P_m\pi^2\left(4+\frac{1}{L^2}\right)\hat{v_1}'. \tag{5.25}$$

Again we note that Equation 5.25 is dependent on $\hat{v_1}'$ only, so this also decouples from the system. It has a similar decaying solution to v_2' in Equation 5.19.

This leaves us with two coupled systems: one involving A_1 and B_2, and one involving A_2 and B_1. Since B_2 is anti-symmetric about the equator and A_1 is symmetric, we call this a 'dipolar mode'. The other system is the converse of this, and we call this a 'quadrupolar mode'. Initially we shall consider the former:

$$\frac{d\hat{A}_1}{dt} = \frac{1}{2}\hat{B}_2 - \pi^2\left(1+\frac{1}{L^2}\right)\hat{A}_1, \tag{5.26}$$

$$\frac{d\hat{B}_2}{dt} = \frac{8D}{3L}\hat{A}_1 - \pi^2\left(1+\frac{4}{L^2}\right)\hat{B}_2. \tag{5.27}$$

We let

$$\hat{A}_1 = A_1e^{st}, \tag{5.28}$$

and

$$\hat{B}_2 = B_2e^{st}, \tag{5.29}$$

where $s \in \mathbb{C}$. Then we proceed with the same method as in Section 3.4, by substituting these forms of $\hat{A}_1$ and $\hat{B}_2$ into Equations 5.26 and 5.27, and representing the system as a matrix equation:

$$\begin{pmatrix} s+\pi^2\left(1+\frac{1}{L^2}\right) & -\frac{1}{2} \\ -\frac{8D}{3L} & s+\pi^2\left(1+\frac{4}{L^2}\right) \end{pmatrix}\begin{pmatrix} A_1 \\ B_2 \end{pmatrix} = \begin{pmatrix} 0 \\ 0 \end{pmatrix}. \tag{5.30}$$

For this equation to hold then the determinant must equal zero, i.e.,

$$0 = \left(s + \pi^2\left(1 + \frac{1}{L^2}\right)\right)\left(s + \pi^2\left(1 + \frac{4}{L^2}\right)\right) - \frac{4D}{3L} \tag{5.31}$$

$$\Rightarrow \quad s = -\pi^2\left(1 + \frac{5}{2L^2}\right) \pm \sqrt{\frac{4D}{3L} + \frac{9}{4L^4}}, \tag{5.32}$$

The state is unstable when $s > 0$, so the critical dynamo number occurs when $s = 0$:

$$D_{crit} = \frac{3\pi^4 L}{4}\left(1 + \frac{5}{2L^2}\right)^2 - \frac{27}{16L^3}. \tag{5.33}$$

If we let $L = 10$, then

$$D_{crit} = 767.55. \tag{5.34}$$

If we repeat the calculation on the quadrupolar system, we obtain a value of

$$D_{crit} = -767.55. \tag{5.35}$$

In order to test the validity of this solution, we can solve Equations 5.13 - 5.17 numerically using a second-order Adams-Bashforth time-stepping method in Matlab (see Section 6). We let $L = 10$ and $P_m = 1$. We set initial conditions of $B_n = 1$ and $A_n = v_n' = 0$ $(n = 1, 2)$, though it turns out the results are insensitive to the choice of initial values. By plotting the solutions for B_1 arising from the usage of $D = -768.5$ (Figure 7) and $D = -767$ (Figure 8), we see that dynamo action occurs for values of $|D| > 767.55$, as expected. Hence the numerics agree with our analytic solution.

In Figure 9 we observe the solutions for $D = -900$. The dipolar mode decays for negative dynamo numbers as expected, whilst the quadrupolar mode evolves into a steady solution. If we were to plot the poloidal potentials A_n for the same dynamo number, we would observe the modes behaving the opposite way to their respective toroidal counterparts. Using a positive dynamo number would have the opposite effect.

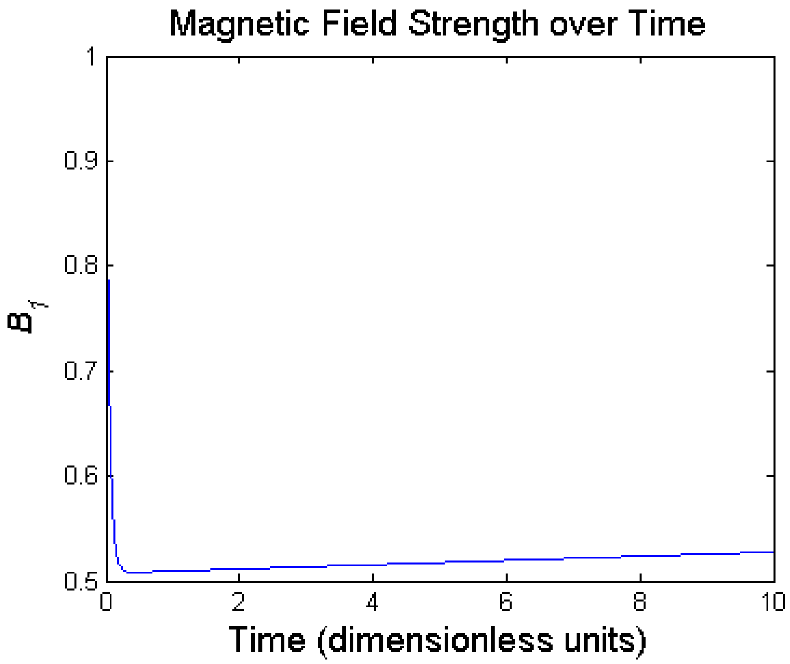

Figure 7: Magnetic field strength over time for $D = -768.5$. Field strength increasing corresponds to dynamo action occurring

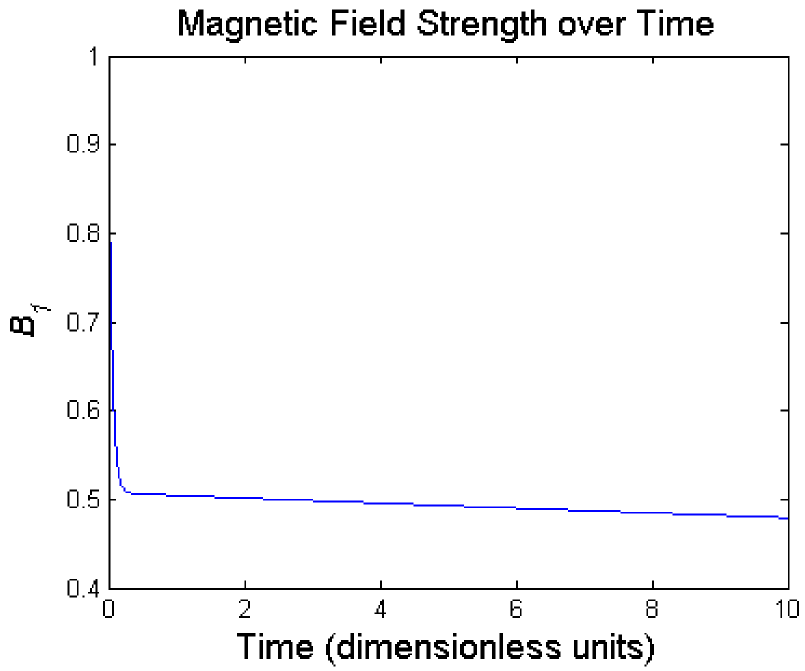

Figure 8: Magnetic field strength over time for $D = -767$. Field strength decreasing corresponds to dynamo action failing

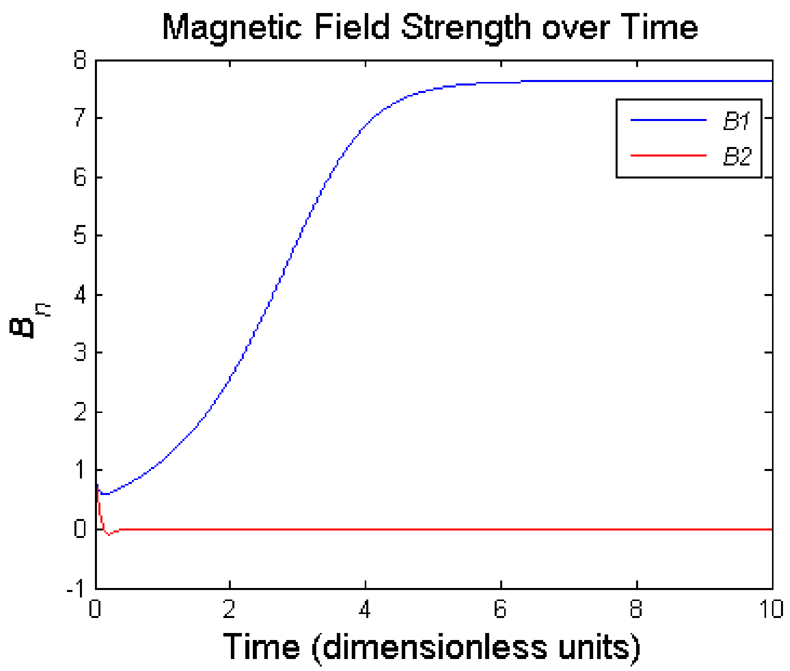

Figure 9: Magnetic field strength over time for $D = -900$. B_1 evolves into a steady mode whilst B_2 decays

We can now begin to add more modes to the Fourier expansions of A, B and v', and repeat the steps above to find the critical dynamo number for each system. As mentioned above, adding more modes should produce more accurate solutions, and hence a more accurate critical dynamo number. Furthermore, in the two-mode case we only find steady modes at onset when we are actually seeking oscillatory dynamo action. To achieve this we set $s = i\omega$, where $\omega > 0$ and $\omega \in \mathbb{R}$. Performing the calculations becomes analytically more complex for $N > 3$, so we can create a program in Matlab which calculates the matrix of linearised coefficients, and solves the characteristic polynomial for D. We let $L = 10$ throughout, and restrict D to negative values (see Section 7). Table 1 shows the critical dynamo numbers for increasing values of N in the dipolar system, as well as the frequency ω.

N	D_{crit}	ω
4	-237.26	4.08
6	-303.25	5.94
8	-364.94	7.33

Table 1: Critical dynamo numbers for the oscillatory modes for increasing N. The value of D_{crit} could be converging as more modes are added

It appears that the critical dynamo number starts to slowly converge as we increase the number of modes in the Fourier series. It seems reasonable to predict that the value of convergence will be somewhere in the range of 400-450. The values for ω suggest a rapid frequency of oscillation, though the frequency could also be converging with D_{crit}. With more time, and better computing power, this could be investigated further.

A possible explanation for this slow convergence lies in the fact that our shear is not dependent on x. This means that we are in effect representing terms like $\cos\left(\frac{n\pi x}{L}\right)$ ($n \in \mathbb{Z}$) as a Fourier sine series in the ODE model, which could lead to slow convergence.

6 Numerical Method

We now use a second-order Adams-Bashforth time-stepping method in Fortran to solve Equations 4.10 - 4.12 numerically. This is of the form:

$$u_{i+1} = u_i + \frac{\delta t}{2}\left(3f_i - f_{i-1}\right), \tag{6.1}$$

where $\frac{\partial u_j}{\partial t} = f_j\left(u_1\left(x,t\right), \ldots, u_J\left(x,t\right), x, t\right), j = 1, \ldots, J$ is the set of J coupled partial differential equations and δt is the time-step. To express the spatial derivatives, we use second-order centred-difference approximations:

$$\frac{\partial u_i}{\partial x} = \frac{u_{i+1} - u_{i-1}}{2\delta x}, \tag{6.2}$$

$$\frac{\partial^2 u_i}{\partial x^2} = \frac{u_{i+1} - 2u_i + u_{i-1}}{\delta x^2}, \tag{6.3}$$

where δx is the grid size. In this case we have $n = 500$ grid points and 10^6 time-steps in order to satisfy the stability condition (Press *et al.*, 1992):

$$\delta t \leq K\delta x^2, \tag{6.4}$$

where K is a constant.

We discretise the model onto a 1D mesh: $0 \leq x \leq 10$. The upper value is chosen so that the strip of the convection zone we are modelling over is suitably rectangular. We set boundary conditions of $A = B = v' = 0$ at $x = 0$ and $x = 10$. Initially we let $D = -500$. We will vary some of these parameters in Section 7.

After solving the equations and plotting the solutions in Matlab, we obtain the contour plot for the toroidal field shown in Figure 10. The light and dark bands represent opposite magnetic polarities, and we see that these reverse after each cycle. Furthermore, the polarity is anti-symmetric about the equator ($x = 5$), which is what we observe on the Sun. Another key feature is the migration of magnetic field (and therefore sunspot emergence) towards the equator, which is what we see in the butterfly diagram in Figure 4.

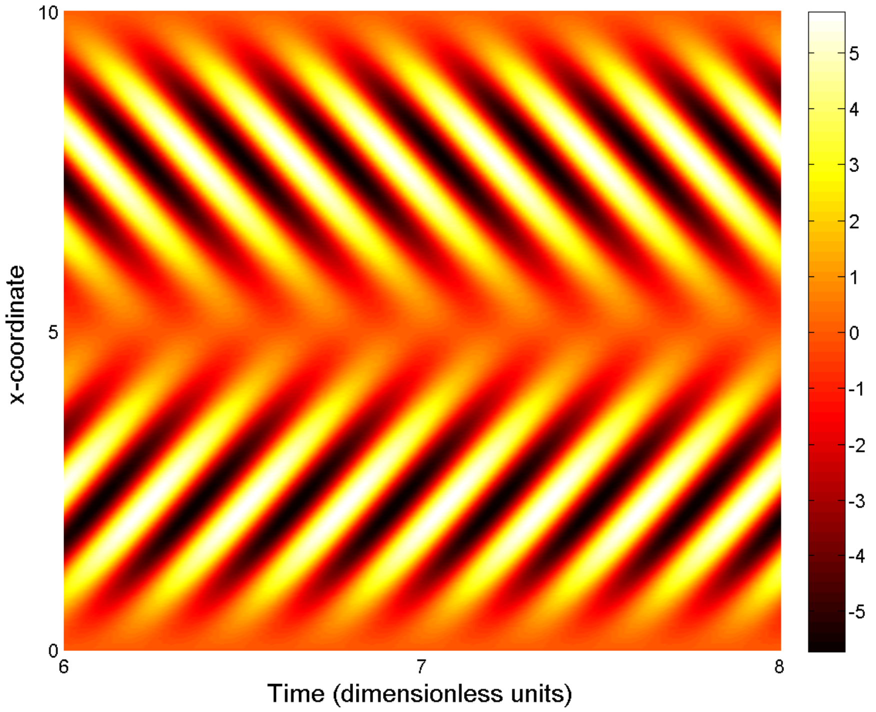

Figure 10: Contour plot of the toroidal field against position and time for $P_m = 1$, $D = -500$. Light and dark areas represent opposite polarities. The field migrates towards the equator over time, mimicking the butterfly diagram

It appears that our simplified, idealised model has replicated many features we observe in the solar magnetic cycle, but has not included modulation in both amplitude and polarity that were discussed in Section 1.2. In Section 7 we will look at how altering the parameters in the model can satisfy these features, particularly periods of minimum activity such as the Maunder Minimum, and the exclusive occupation of the magnetic field to a single hemisphere after this period.

We will also look at the magnetic and kinetic energies for different values of D and P_m. The magnetic energy is given by the following expression:

$$E_B = \int_V \frac{B^2}{2} \, \mathrm{d}V. \tag{6.5}$$

Since $B \sim B(x,t) \sin(\pi z)$, with $0 \leq z \leq 1$, $0 \leq x \leq L$, the integral becomes:

$$E_B = \frac{1}{2} \int_0^L \int_0^1 B^2(x,t) \sin^2(\pi z) \; \mathrm{d}z \mathrm{d}x. \tag{6.6}$$

Now

$$\begin{aligned} \int_0^1 \sin^2(\pi z) \; \mathrm{d}z &= \frac{1}{2} \int_0^1 1 - \cos(2\pi z) \; \mathrm{d}z \\ &= \frac{1}{2} \left[z - \frac{1}{2\pi} \sin(2\pi z) \right]_0^1 \\ &= \frac{1}{2}, \end{aligned} \tag{6.7}$$

so

$$\frac{1}{2} \int_V B^2 \, \mathrm{d}V = \frac{1}{4} \int_0^L B^2(x,t) \; \mathrm{d}x. \tag{6.8}$$

We can estimate this integral computationally using the Trapezium Rule:

$$E_B \approx \frac{\delta x}{8} \left(B^2(1) + B^2(n) + 2 \sum_{i=2}^{n-1} B^2(i) \right), \tag{6.9}$$

where n is the number of grid points. We maintain consistency by setting $n = 500$.

Similarly $v' \sim v'(x,t) \sin(2\pi z)$, so we can define the kinetic energy as:

$$E_{v'} \approx \frac{\delta x}{8} \left(v'^2(1) + v'^2(500) + 2 \sum_{i=2}^{499} v'^2(i) \right). \tag{6.10}$$

Now using Matlab we can plot the energy change over time.

7 Parameter Survey

In this section we look at how varying parameters in the model affects numerical results. We consider the effect of varying both the dynamo number D, and the Magnetic Prandtl number P_m, which is the ratio of viscosity and magnetic diffusivity.

We begin by trying to find the critical value of D for this model. If $D > 0$ then we observe migration away from the equator (Figure 11), so we restrict D to negative values only. By increasing the number of time units and then using a method of interval bisection by gradually decreasing and increasing the upper and lower bounds of $|D|$ respectively, we observe that dynamo action occurs at a critical value of $D_{crit} \approx -394.8$. For values of $|D|$ smaller than $|D_{crit}|$, the magnetic field appears to decay over time. In Section 5 we predicted $-450 \lesssim D_{crit} \lesssim -400$, so our analytical work seems robust. If we were to add more Fourier modes, we would expect the critical dynamo number to converge to a value of $D_{crit} \approx -394.8$. Based on the eight-mode expansion, this seems plausible.

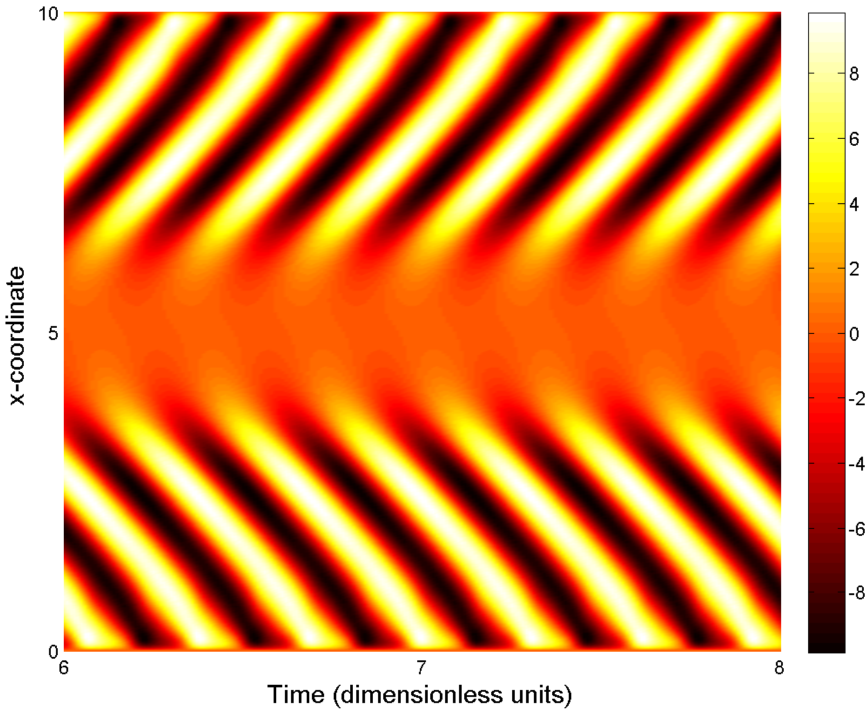

Figure 11: Contour plot of the toroidal field for $P_m = 1$, $D = 1000$. The field migrates away from the equator over time

By setting $P_m = 1$, we can vary D to see how it contributes to modulation. For $D = -500$, we observe the same anti-symmetric pattern seen in Figure 10. This is a dipolar mode (see Section 5), so the parity of the mode is consistent with the system we found a critical dynamo number for. In a dipolar mode, the poloidal potential is symmetric about the equator. In a quadrupolar mode the poloidal potential is equatorially anti-symmetric. Solutions with no clear symmetry are known as 'mixed-parity modes' (Tobias, 1997). This is comparable to the results in Section 5 where we obtained two coupled systems; one was dipolar and the other was quadrupolar at onset.

At $D = -1000$, the solutions are mixed-parity modes (Figure 12), with slight modulation in the magnetic field strength over time. This modulation in amplitude is more evident if we look at the magnetic energy oscillations in Figure 13. The units of energy are dimensionless. Whilst the oscillations seem periodic with a few occasional irregularities, the amplitude also oscillates. If we were to extend the butterfly diagram over a longer time period, we would expect to see lighter and darker regions, corresponding to stronger and weaker magnetic field. This modulation is also apparent in the kinetic energy (Figure 14), where we see a periodic oscillatory pattern with an oscillating amplitude.

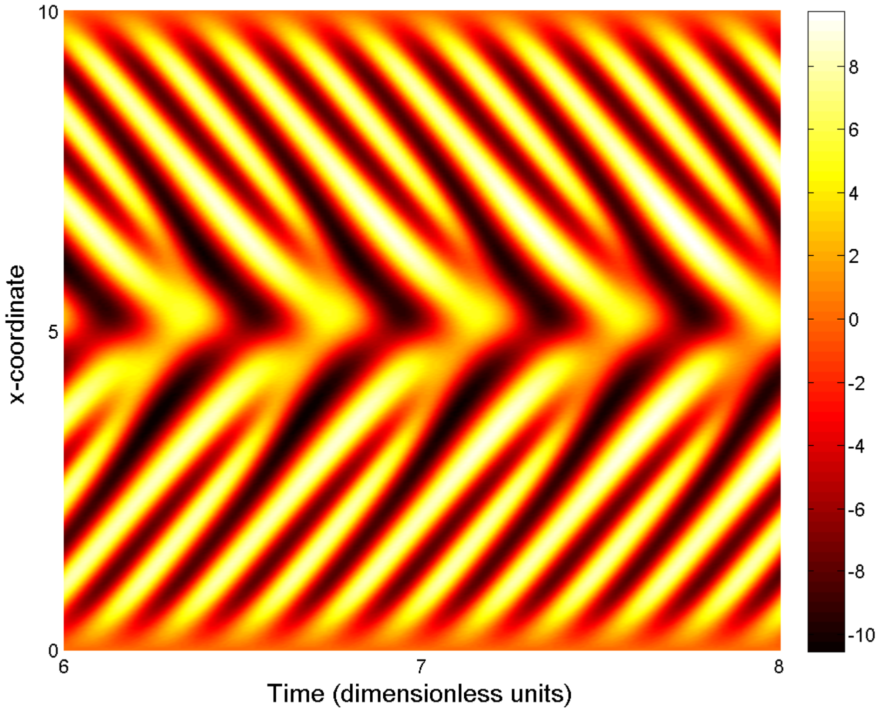

Figure 12: Contour plot of the toroidal field for $P_m = 1$, $D = -1000$. There is evidence of symmetry modulation

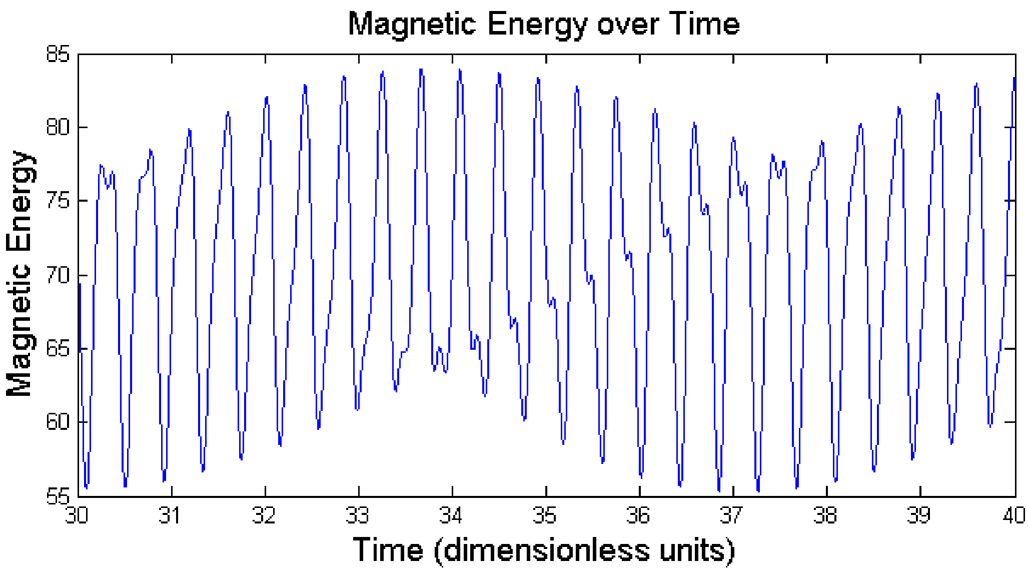

Figure 13: Magnetic energy oscillations for $P_m = 1$, $D = -1000$. Slight modulation in the oscillations is observed, whilst there is an overall variation in amplitude

If we decrease D to be -2000, we observe a nearly quadrupolar mode in Figure 15, except here the positions where the fields in the two hemispheres meet, i.e., the equator, is slightly inconsistent over time. For a quadrupolar mode we would expect this position to be at $x = 5$, but in this case the central position seems oscillatory. This is due to modulation of parity, which occurs because of the interaction of dipolar and quadrupolar modes.

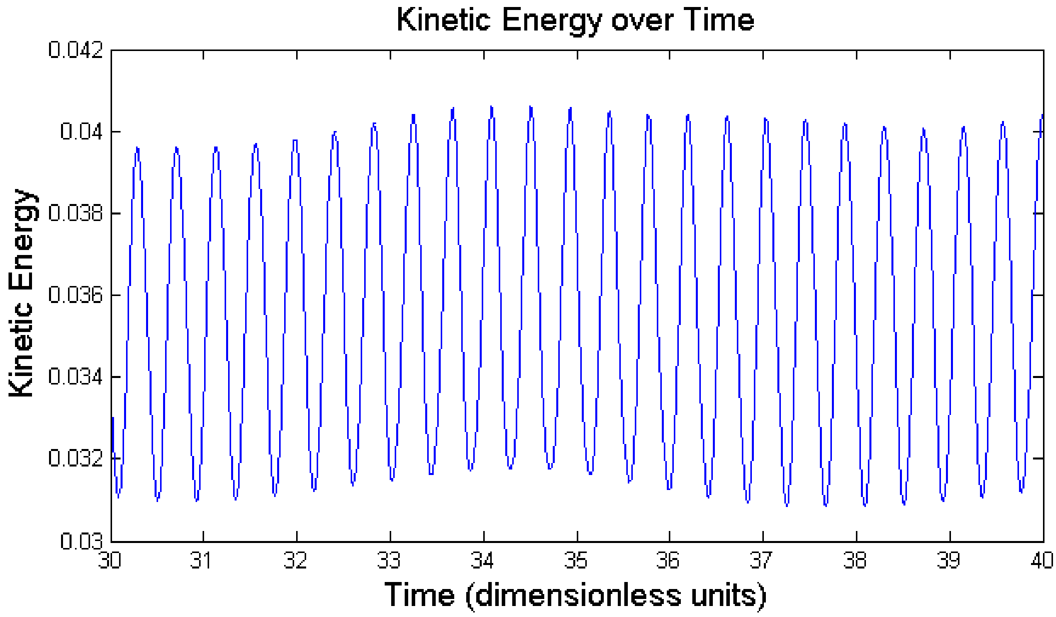

Figure 14: Kinetic energy oscillations for $P_m = 1$, $D = -1000$. As with the magnetic energy, the amplitude also oscillates

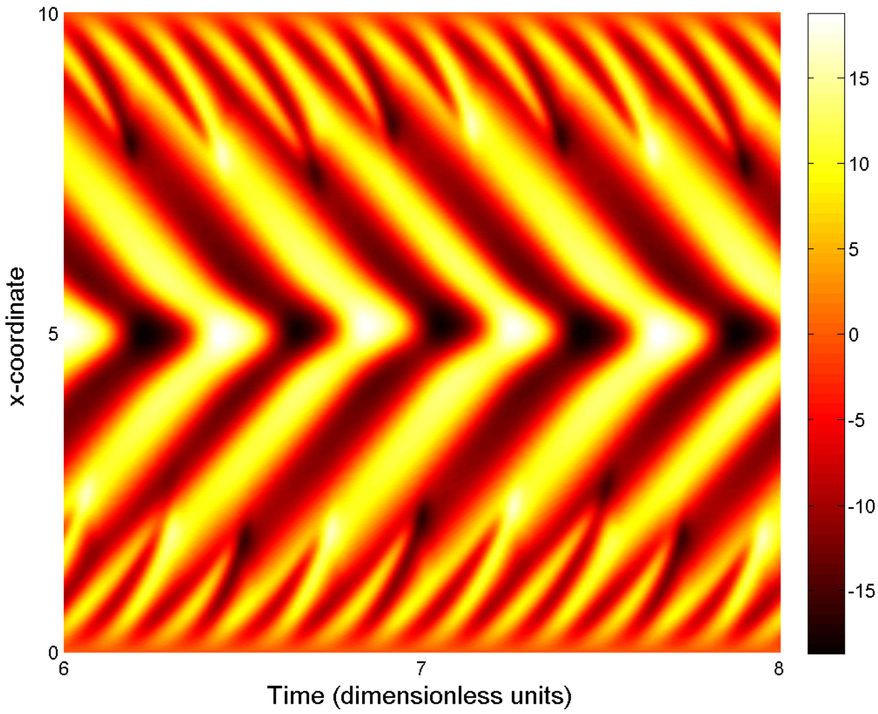

Figure 15: Contour plot of the toroidal field for $P_m = 1$, $D = -2000$. This mode is almost quadrupolar, with a slight parity modulation

Now we look at the plots for $P_m = 0.1$. The Prandtl number affects the timescale of response of velocity perturbations, so decreasing it may lead to modulation of parity and amplitude (Tobias, 1997). For $D = -500$, we again observe a dipolar mode, as in Figure 10. However if we now decrease the dynamo number to -1000, the parity becomes mixed, although almost quadrupolar, and we start to see some periods of strong and weak toroidal field (Figure 16). The energy oscillations become more chaotic (Figure 17), although we can still infer that there is some sort of quasi-periodicity since the envelope of the wave oscillates and consecutive peaks alternate between high and low energy. In fact the amplitude of the 'small' peaks also seems to oscillate. This is easier to see for the kinetic energy in Figure 18. A fast Fourier transform (FFT) of the signal shows three peaks, representing three different frequencies that are present within the signal, enforcing our beliefs of multi-periodicity. Based on this information, we can confidently say that this value of P_m accommodates modulation of both amplitude and parity.

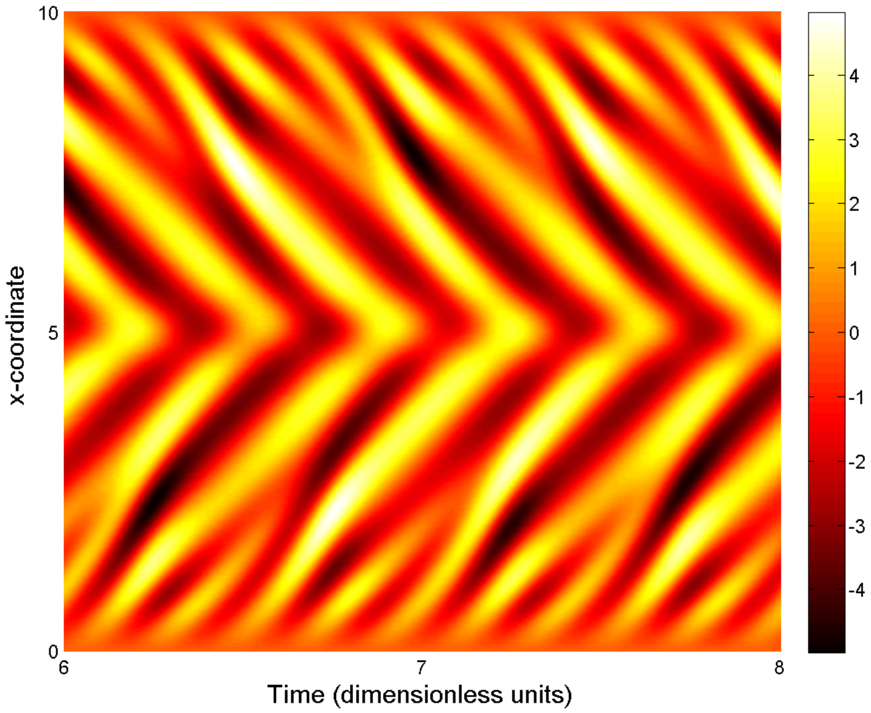

Figure 16: Contour plot of the toroidal field for $P_m = 0.1$, $D = -1000$. Strong modulation in amplitude is observed, whilst the parity is almost quadrupolar

At $D = -2000$, Figure 19 shows that the solutions are not only symmetric about the equator, but also periodic. There is also a stable equatorial position about $x = 5$ in contrast to what was observed in Figure 15. This is what we would expect from a quadrupolar mode.

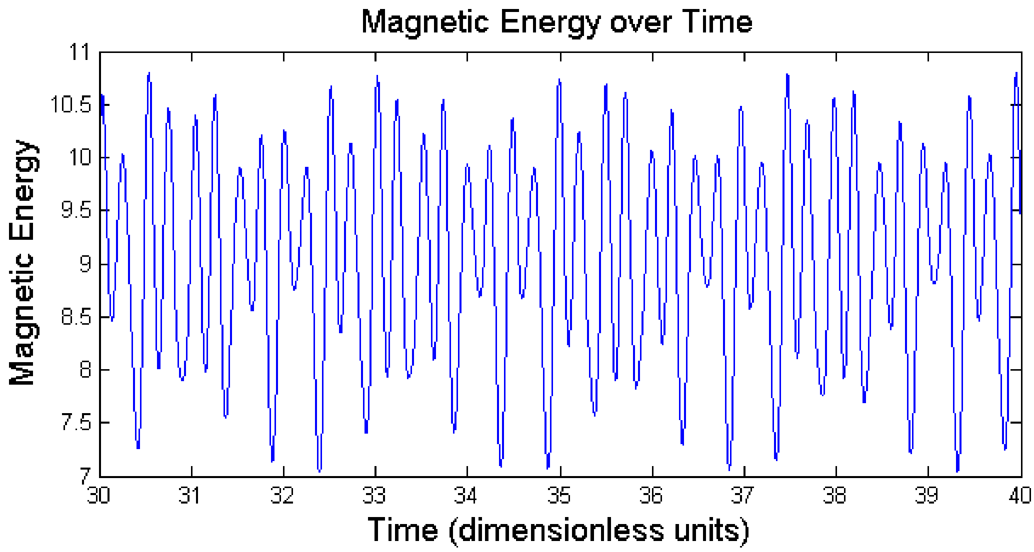

Figure 17: Magnetic energy oscillations for $P_m = 0.1$, $D = -1000$. There is strong amplitude modulation, supporting the butterfly diagram

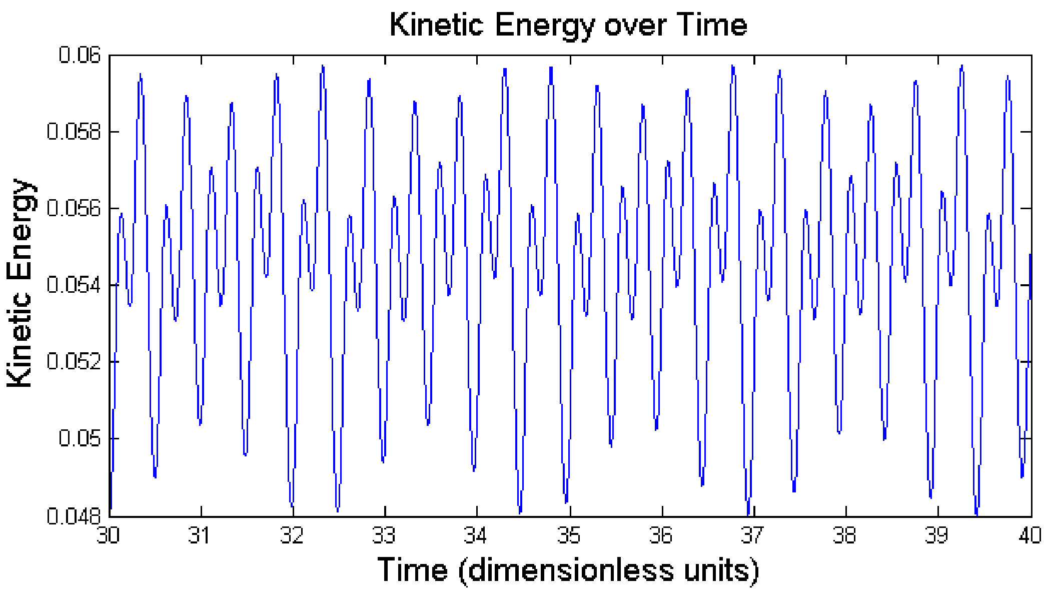

Figure 18: Kinetic energy oscillations for $P_m = 0.1$, $D = -1000$. Again, modulation of amplitude is present

Finally we let $P_m = 0.01$ and return to $D = -500$. In like fashion to higher values of P_m, a dipolar mode is observed in Figure 20, but this time there are periods of lower field strength in the northern hemisphere, indicating potential periods of grand minima, though this could just be due to initial transients.

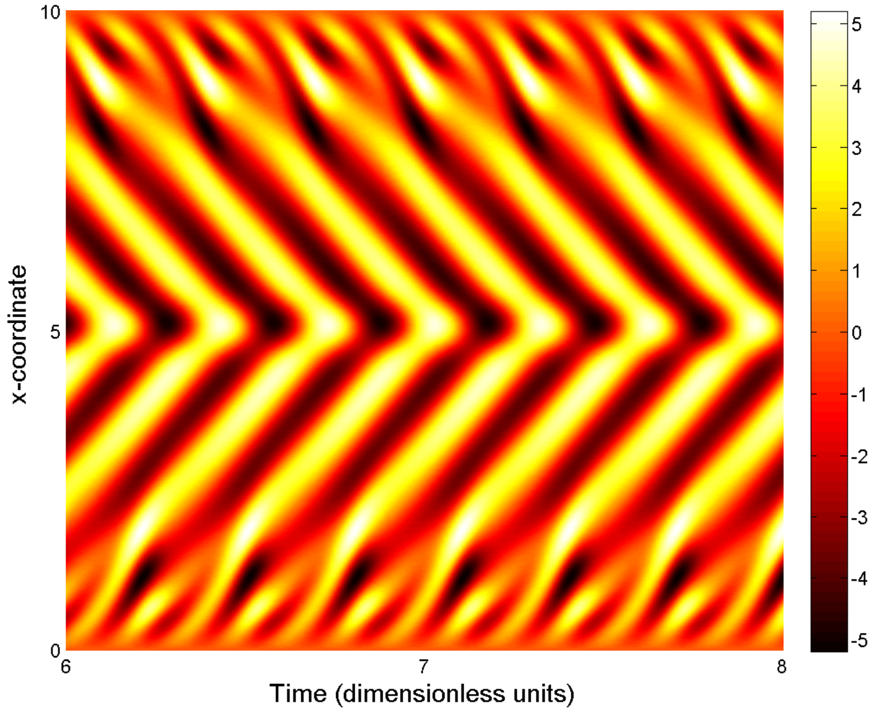

Figure 19: Contour plot of the toroidal field for $P_m = 0.1$, $D = -2000$. The mode is quadrupolar

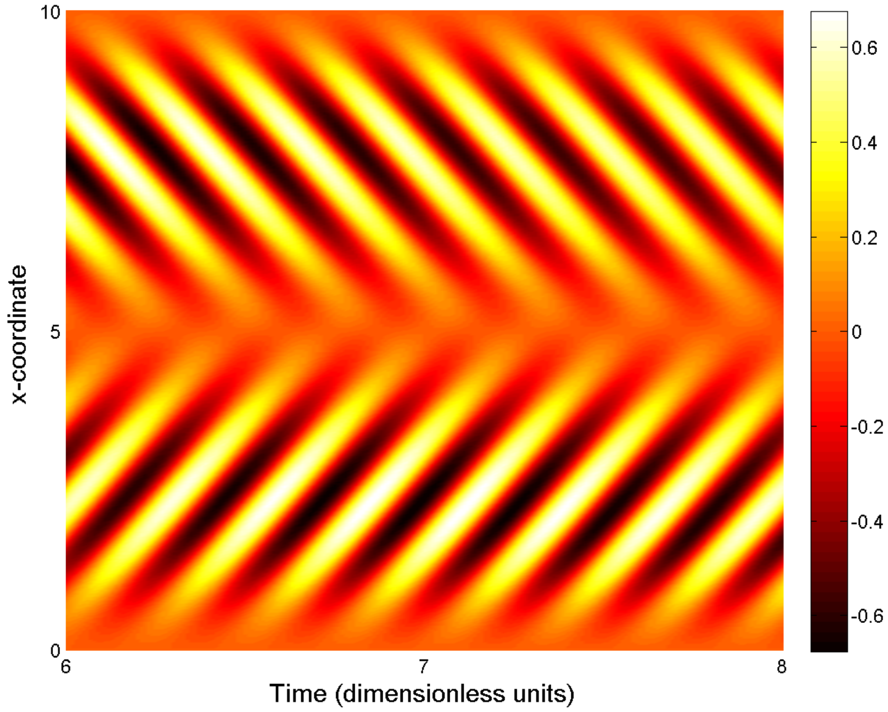

Figure 20: Contour plot of the toroidal field for $P_m = 0.01$, $D = -500$. Almost identical to the plot for $P_m = 1$, except there is a little modulation in the northern hemisphere

If we set $D = -1000$ (Figure 21), we observe a mixed-parity mode, though in this case it is close to being dipolar. The solutions appear to be quasi-periodic, and we see strongly varying toroidal field strength. The more notable of these periods are those of low activity, because they can be compared directly to periods like the Maunder Minimum. The key difference in this case is that there is no clear evidence of a cycle occupying a single hemisphere after a minimum. Modulation is again supported by the plots for the magnetic and kinetic energies (Figures 22 and 23 respectively), except this time we decrease the timescale to fully observe the extent of this modulation. Both plots show seemingly unpredictable amplitudes, though the peaks occur at almost regular intervals.

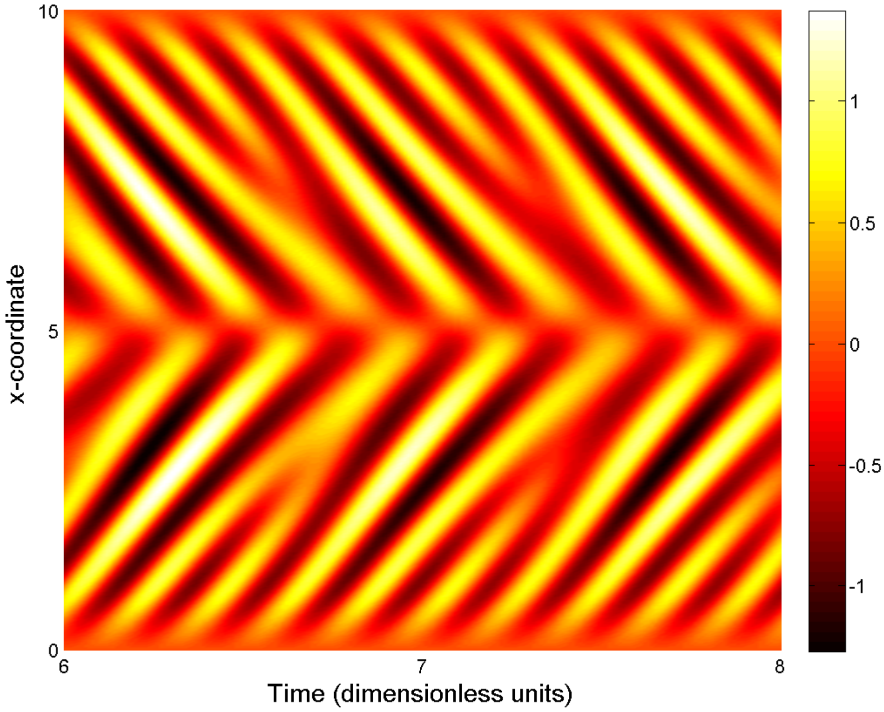

Figure 21: Contour plot of the toroidal field for $P_m = 0.01$, $D = -1000$. It is a dipolar mode with periods of varying magnetic field strength

At $D = -2000$, the mode seems to be quadrupolar (Figure 24), and again we see periods of high and low magnetic activity. It could be suggested that decreasing D from -500 to -2000 shifts the field from a dipolar to quadrupolar mode, and decreasing the Magnetic Prandtl number introduces modulation of amplitude. With more time available, these suggestions could be explored further.

It also appears that the frequency decreases as the Magnetic Prandtl number decreases. Decreasing P_m corresponds to decreasing the viscous diffusion rate, which allows for a greater velocity perturbation. This perturbation then hinders the dynamo and its associated oscillations, including magnetic and kinetic energy, so the frequencies of these oscillations decrease.

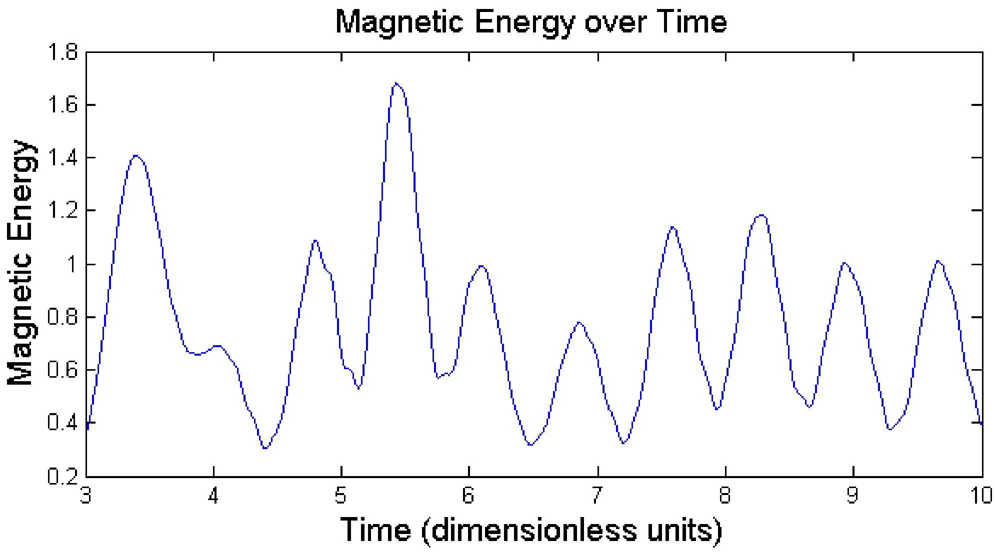

Figure 22: Magnetic energy oscillations for $P_m = 0.01$, $D = -1000$. Strong modulation in amplitude is evident; oscillations have become very irregular

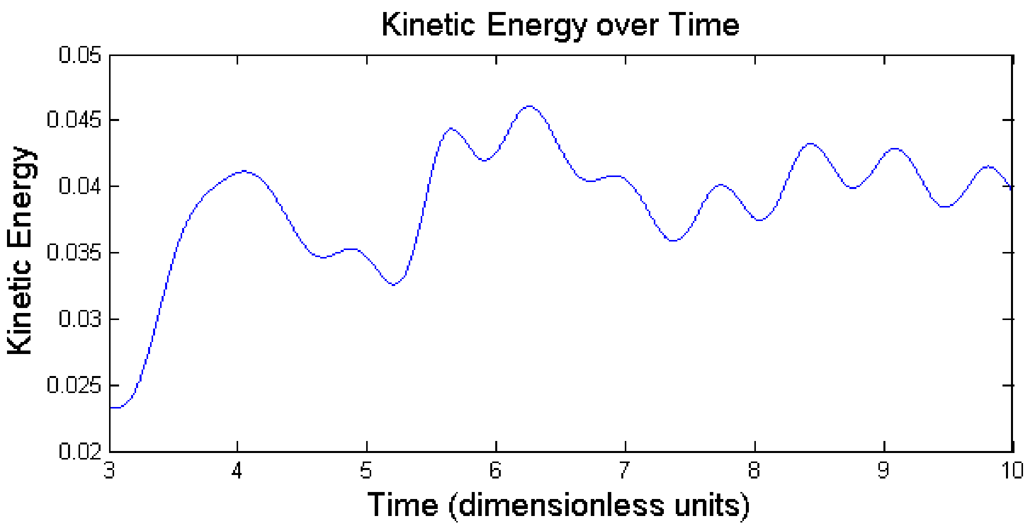

Figure 23: Kinetic energy oscillations for $P_m = 0.01$, $D = -1000$. Strong modulation is also observed

By considering the average energy over time, we can see how decreasing P_m for given values of D affects the average amplitude of the oscillations. Figure 25 shows the trend of average magnetic energy for different values of the dynamo number, given five calculated values of average energy from increasing values of the Magnetic Prandtl number. For each value of D the average energy decreases as P_m decreases. This is to be expected, as we know decreasing P_m increases the velocity perturbation. This in turn inhibits magnetic activity, so the magnetic energy is lower.

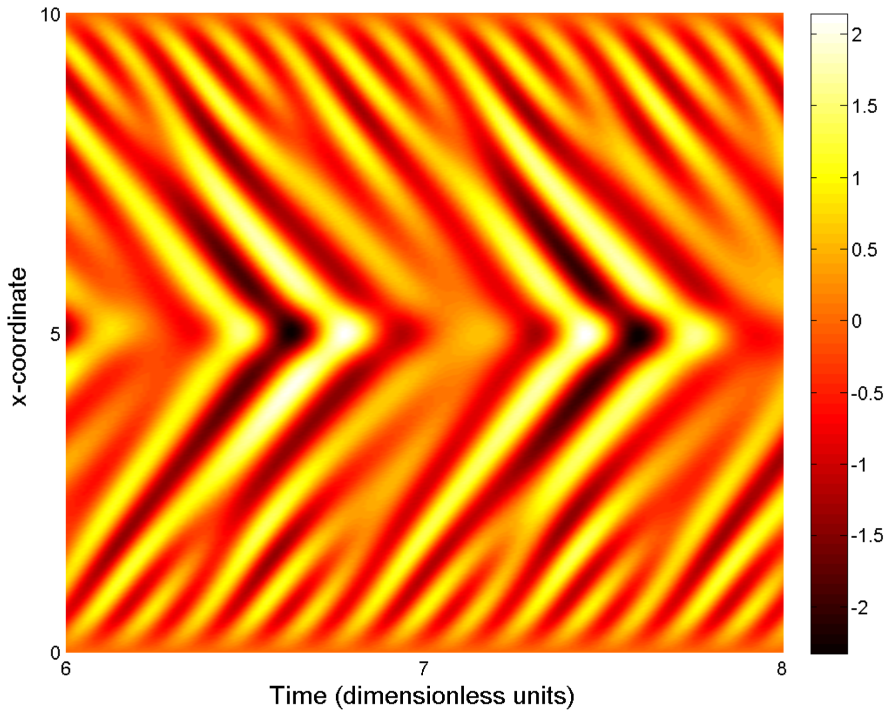

Figure 24: Contour plot of the toroidal field for $P_m = 0.01$, $D = -2000$. The field is almost quadrupolar, and there is also amplitude modulation

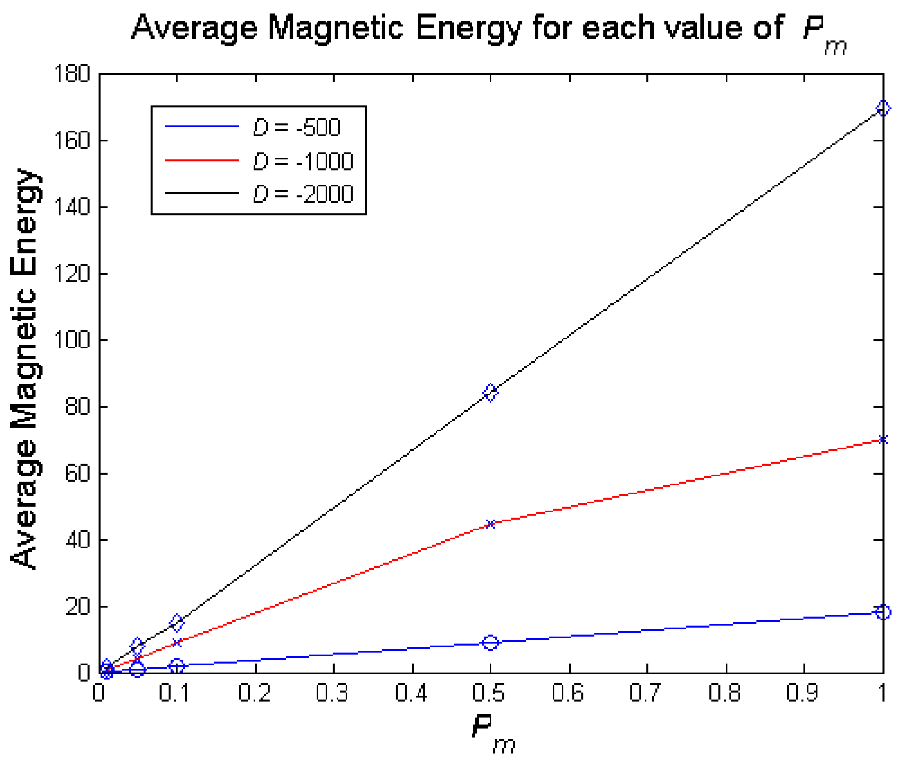

Figure 25: Average magnetic energy for increasing P_m. Values were calculated at $P_m = 0.01, 0.05, 0.1, 0.5, 1$. There is a positive correlation for each value of D

Figure 26 shows the equivalent plot for the average kinetic energy. In this case the energy increases sharply for low values of P_m, before reaching a certain value of P_m and then decreasing as the parameter is increased. However it isn't entirely clear why this pattern occurs. We would expect the energy to decrease throughout, since increasing P_m would increase viscosity, inhibiting the growth of momentum and kinetic energy. However at very small values of the Prandtl number, the kinetic energy growth will depend solely on the magnetic fields generated by the dynamo. This is easier to understand by looking at Equation 4.12. A small value of P_m would mean the generated velocity field relies on the nonlinear term relating to the Lorentz force. Increasing P_m would then include a new source from existing velocity field which would contribute to the overall kinetic energy. Eventually the Prandtl number would be increased to a value where viscosity would start to have an effect as discussed above.

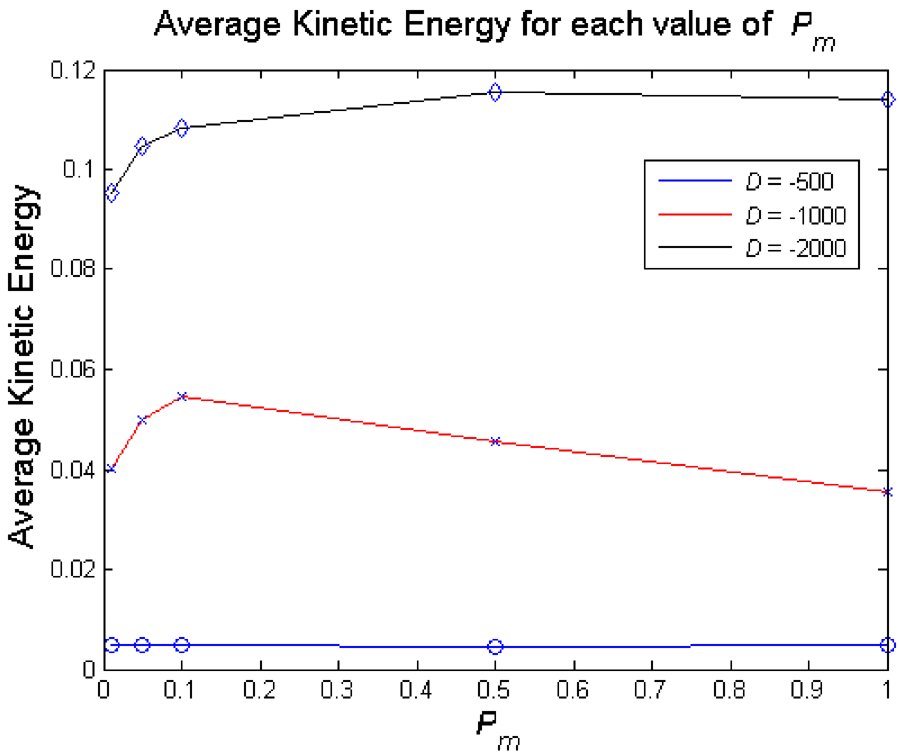

Figure 26: Average kinetic energy for increasing P_m. For each value of D there is an initial increase in energy before settling to a downward trend

This parameter sweep has investigated the effect of parameters on both modulation and energy. We have found values of D which produce both dipolar and quadrupolar modes, as well as modes of mixed-parity. Combinations of high values of $|D|$ and low values of P_m have generated solutions which include modulation in amplitude, showing periods of low and high magnetic activity. The value of $P_m = 0.01$ in particular provided strongly modulated energy oscillations.

8 Conclusions and Future Work

We set out with the aim of producing a mathematical model for the solar dynamo which would replicate observations discussed in Section 1.2. By making various simplifying assumptions and setting justifiable forms of the magnetic and velocity field components, we were able to construct a dimensionless nonlinear PDE model which could be solved numerically.

We then reduced this model to a system of ODEs by considering Fourier sine series expansions. The ODE model separated into two coupled equations and, starting with $N = 2$ modes and adding an extra mode each time, we were able to calculate the critical dynamo number for the system. We hoped that the value of D_{crit} would converge quickly, but even after eight modes had been included the rate of convergence was still slow. This may be attributed to the functional dependence of the shear. Furthermore, every time a mode was added the matrix entries took longer to compute and the characteristic polynomial took longer to solve. In order for the converged value of D_{crit} to be found, a lot more time and potentially a better computer would have been required. This is still an area of interest and could be looked into in future work.

We returned to the PDE model and, noting that we required $D < 0$ to ensure equatorward migration of magnetic field, found a value of $D_{crit} \approx -394.8$, which was qualitatively consistent with the prediction made in Section 5. The plot of the results (Figure 10) included features observed on the Sun, such as equatorward migration and anti-symmetry in polarity about the equator. However it didn't include modulation in either amplitude or symmetry which are both observed on the Sun, particularly during and after periods of grand minima. The remainder of the project was dedicated to varying the parameters D and P_m in order to account for this modulation.

Values of $P_m = 1, 0.1, 0.01$ and $D = -500, -1000, -2000$ were applied, and their effects on both the butterfly diagram and magnetic and kinetic energy plots were analysed. We found that decreasing the dynamo number seemed to shift the field from a dipolar to an almost quadrupolar mode, with the intermediate values producing mixed-parity modes, accounting for modulation of symmetry. Decreasing the Magnetic Prandtl number introduced amplitude modulation, which was easier seen in the energy plots, particularly for $P_m = 0.01$, where strong modulation was observed. We also investigated the effect of the Prandtl number on average energy, and found that generally the average magnetic energy decreases and the average kinetic energy increases as P_m decreases. This was not always the case, however, and future research could involve giving P_m and D a much larger range of values to extract the overall effect these parameters have on the model. In order to produce a more accurate model for the solar dynamo, the parameters should be fixed to obtain the desired features of the solar magnetic field.

Another possibility for future progress is performing centre manifold reductions on the system (following a similar method to Bushby (2003)) to reduce it to a system of just two ODEs, which could be solved analytically. The oscillatory case could also be reduced, producing a system of four equations to be solved either numerically or analytically and compared to the solutions from Section 5, though the complexity of the algebra is currently unclear. Given the ever-increasing modern-day computing power and the understanding of the importance of studying the Sun's magnetic field, the future of solar dynamo research appears to be very promising, with endless possibilities for direction.

9 Appendix

In Sections 3.1 and 3.2 we used two identities from vector calculus. This appendix shows the proofs of these identities using suffix notation.

a) We have

$$[\nabla \times (\nabla \times \mathbf{A})]_i = \epsilon_{ijk} \frac{\partial}{\partial x_j} [\nabla \times \mathbf{A}]_k \tag{9.1}$$

$$= \epsilon_{ijk} \frac{\partial}{\partial x_j} \epsilon_{kpq} \frac{\partial}{\partial x_p} A_q \tag{9.2}$$

$$= \epsilon_{kij} \epsilon_{kpq} \frac{\partial}{\partial x_j} \frac{\partial}{\partial x_p} A_q \tag{9.3}$$

$$= (\delta_{ip}\delta_{jq} - \delta_{iq}\delta_{jp}) \frac{\partial}{\partial x_j} \frac{\partial}{\partial x_p} A_q \tag{9.4}$$

$$= \frac{\partial}{\partial x_j} \delta_{ip} \frac{\partial}{\partial x_p} \delta_{jq} A_q - \frac{\partial}{\partial x_j} \delta_{jp} \frac{\partial}{\partial x_p} \delta_{iq} A_q \tag{9.5}$$

$$= \frac{\partial}{\partial x_j} \frac{\partial}{\partial x_i} A_j - \frac{\partial}{\partial x_j} \frac{\partial}{\partial x_j} A_i \tag{9.6}$$

$$= \frac{\partial}{\partial x_i} \left(\frac{\partial A_j}{\partial x_j} \right) - \frac{\partial^2}{\partial x_j \partial x_j} A_i \tag{9.7}$$

$$= \left[\nabla (\nabla \cdot \mathbf{A}) - \nabla^2 \mathbf{A} \right]_i . \tag{9.8}$$

Hence $\nabla \times (\nabla \times \mathbf{A}) = \nabla (\nabla \cdot \mathbf{A}) - \nabla^2 \mathbf{A}$ as required.

b) We have

$$[\nabla \times (\phi \mathbf{A})]_i = \epsilon_{ijk} \frac{\partial}{\partial x_j} (\phi A_k) \tag{9.9}$$

$$= \phi \epsilon_{ijk} \frac{\partial A_k}{\partial x_j} + \epsilon_{ijk} \left(\frac{\partial \phi}{\partial x_j} \right) A_k \tag{9.10}$$

$$= \phi [\nabla \times \mathbf{A}]_i + [(\nabla \phi) \times \mathbf{A}]_i . \tag{9.11}$$

Hence $\nabla \times (\phi \mathbf{A}) = \phi \nabla \times \mathbf{A} + (\nabla \phi) \times \mathbf{A}$ as required.

References

Beer, J. 2000 Long-term indirect indices of solar variability. *Space Science Reviews* **94**, 53–66.

Beer, J., Tobias, S. & Weiss, N. 1998 An Active Sun Throughout the Maunder Minimum. *Solar Physics* **181**, 237–249.

Bushby, P. & Mason, J. 2004 Solar dynamo: Understanding the solar dynamo. *Astronomy and Geophysics* **45** (4), 7.

Bushby, P. J. 2003 Strong asymmetry in stellar dynamos. *Monthly Notices of the RAS* **338**, 655–664.

Eddy, J. A. 1976 The Maunder Minimum. *Science* **192**, 1189–1202.

Hale, G. E. 1924 The Law of Sun-Spot Polarity. *Proceedings of the National Academy of Science* **10**, 53–55.

Hoyt, D. V. & Schatten, K. H. 1997 *The Role of the Sun in Climate Change*. Oxford University Press.

Parker, E. N. 1955*a* Hydromagnetic Dynamo Models. *Astrophysical Journal* **122**, 293.

Parker, E. N. 1955*b* The Formation of Sunspots from the Solar Toroidal Field. *Astrophysical Journal* **121**, 491.

Press, W. H., Teukolsky, S. A., Vetterling, W. T. & Flannery, B. P. 1992 *Numerical Recipes in FORTRAN. The Art of Scientific Computing*. Cambridge University Press.

Schou, J. *et al.* 1998 Helioseismic Studies of Differential Rotation in the Solar Envelope by the Solar Oscillations Investigation Using the Michelson Doppler Imager. *Astrophysical Journal* **505**, 390–417.

Spiegel, E. A. & Zahn, J.-P. 1992 The solar tachocline. *Astronomy and Astrophysics* **265**, 106–114.

Tobias, S. M. 1996 Grand minimia in nonlinear dynamos. *Astronomy and Astrophysics* **307**, L21.

Tobias, S. M. 1997 The solar cycle: parity interactions and amplitude modulation. *Astronomy and Astrophysics* **322**, 1007–1017.

Tobias, S. M. 2002 The solar dynamo. *Royal Society of London Philosophical Transactions Series A* **360**, 2741–2756.

Tobias, S. M., Brummell, N. H., Clune, T. L. & Toomre, J. 1998 Pumping of Magnetic Fields by Turbulent Penetrative Convection. *Astrophysical Journal, Letters* **502**, L177–L180.